FINAL TECHNICAL REPORT

Novel Electrically Small Antennas and Metamaterial High Impedance Surfaces

June 2004–September 2005

Submitted to

Office of Naval Research

Grant number: *N00014-04-1-0619*

Principal Investigator

Ahmad Hoorfar

Contributors

Prof. Ahmad Hoorfar
Mr. John McVay
Ms. Jinhui Zhu
Mr. Hui Huang

December 2005

Table of Contents

1. Summary

This final report presents a summary of the work performed on the project *"Novel Electrically Small Antennas and Metamaterial High Impedance Surfaces,"* under ONR Grant No. N00014-04-1-0619, over the period of June 1, 2004 to September 30, 2005.

The main accomplishments are:

1. Investigation of fundamental characteristics of matched off-center fed Space-Filling Curve (SF-Curve) radiating elements such as Hilbert curve and Peano curve antennas for low-frequency applications, and fabrication and measurement of a prototype to verify the theory.

2. Analysis of mutual coupling effects between a pair of SF-curve antennas, and investigation of Yagi arrays made of Peano or Hilbert antenna elements.

3. Analysis of high-impedance surfaces (ground-planes), also known as artificial magnetic conductors (AMC), made of a periodic arrangement of inclusions made of Hilbert or Peano scattering elements, fabrication and measurement of a Hilbert AMC surface.

4. Application of SF-curve AMC surfaces in design of electrically thin microwave absorbers for RCS reduction, and analysis and RCS measurement of a rectangular conducting plate covered by such a surface to confirm the theory.

5. Application of an array made of SF-curve resonating elements in design of novel RFID tags, and their performance analysis in RF tagging of dielectric and conducting cylindrical objects.

In Section 2, we present analysis and measurement of SF-curve antenna elements. Section 3 presents the results on mutual-coupling effects, and optimization of Yagi arrays of the Hilbert and Peano elements. In Section 4, we present the analysis and measurement of AMC surfaces made of SF-curve inclusions and their application in design of thin

absorbers. Finally, in Section 5 analysis and scattering performance of Hilbert and Peano RF tags are presented.

Publications based on this research grant

1. J. Zhu, A. Hoorfar, N. Engheta, "Peano Antennas", *IEEE Antennas and Wireless Propagation Letters*, Vol. 3, PP. 71-74, December 2004.

2. J. McVay, A. Hoorfar and N. Engheta, "Peano High Impedance Surfaces," *Radio Science*, Vol. 40, pp. 1-9, September 2005.

3. J. McVay, A. Hoorfar and N. Engheta, "Space-Filling-Curve High-Impedance Ground Planes," accepted for *Wiley Publications* as a Chapter for a book on Metamaterials.

4. R. Komanduri, A. Hoorfar and F. Plonski, "Performance Analysis of a Dual Stacked E-Shaped Patch Antenna on a USV Platform for Broadband VHF Applications", Proceedings of *Intelligent Ship Symposium*, June 2005.

5. J. Zhu, A. Hoorfar, N. Engheta and F. Plonski, "Miniaturized Antennas for Low Frequency Applications", Proceedings of *Intelligent Ship Symposium*, June 2005.

6. J. McVay, A. Hoorfar and N. Engheta, "Techniques for Bandwidth Enhancement and Polarization Dependence Reduction of Space-Filling Curve Artificial Magnetic Conductors," *IEEE International Symp. on Antennas and Prop.*, and URSI Meeting, July 2005.

7. J. McVay, N. Engheta and A. Hoorfar, "Radio Frequency Identification Utilizing Passive Space-Filling Curves," *IEEE International Symp. on Antennas and Prop., and URSI Meeting*, July 2005.

8. J. McVay, A. Hoorfar and N. Engheta,"Thin Absorbers Using Space-Filling Curve High Impedance Surfaces," Proceedings of *IEEE International Symposium on Antennas and Propagation*, July 2005.

9. J. McVay, N. Engheta and A. Hoorfar, "Numerical Study and Parameter Estimation for Double-Negative Metamaterials with Hilbert-Curve Inclusions," Proceedings of *IEEE International Symposium on Antennas and Propagation*, July 2005.

10. N. Engheta and A. Hoorfar and J. McVay, "Electrodynamics of Space-Filing Curves," Proceedings of *International Conference on Electromagnetics in Advanced Applications*, Turin, Italy, September 2005.

11. J. McVay, N. Engheta and A. Hoorfar," Numerical Study of Phase Variation through Double Negative and Single-Negative Media Formed by Space-filling Curve Inclusions," Proceedings of *International Conference on Electromagnetics in Advanced Applications*, Turin, Italy, September 2005.

2. Space-filling Curve Antenna Elements

In recent years, there has been a considerable interest in the development of low profile electrically small antennas for both the civilian as well as the military applications. Low-profile antenna systems are of crucial importance in a wide range of applications including portable voice and data communication systems, commercial and military radar, and digital battlefields. In particular, designs of low-profile electrically small antennas are of paramount importance in such low-frequency on-board Department of Defense (DoD) applications as PRC-5 VHF (33-88MHz, and 135-175MHz), Military UHF COMMS (225-400MHz), TCAS/ IFF (1030-1090 MHz) and TACAN/DME (962-1252 MHz). Conventional wire dipole and monopole antennas are still widely used in low-frequency military applications for voice, data, telemetry, direction finding and other usages on tanks, ships, aircrafts and unmanned autonomous and surface vehicles (UAV and USV). Size and weight of the antennas are of particular concern in the latter two applications where low profile, low weight and low observable radiating elements are desired.

In this section we will present an overview of our research results on the use of the mathematical concept of space-filling curves [1], such as Hilbert and Peano curves, to develop electrically small antennas for potential applications in low frequency systems discussed above. Space–filling curves are, in general, a continuous mapping from a normalized one-dimensional [0, 1] interval to a normalized two-dimensional (2-D) region, $[0, 1]^2$, passing through every point in the region as one increases the iteration order of the curve from 1 to infinity. Since Peano demonstrated the construction of the first space-filling curve in 1890, many such curves have been suggested over the years [1]. One of the most widely used of such curves is the one proposed by David Hilbert in 1891. The Hilbert curves for the first few iteration orders are shown in Fig. 1. The plane-filling nature is evident by comparing the first few iteration stages. It is clear that as the iteration order increases, the total length of the line segments is increased in almost geometric progression if the side outer dimension of its "foot print" is kept fixed. For a Hilbert curve with side dimension L and order n, the length of each line segment d and

5

the sum of all the line segments S_h are given by,

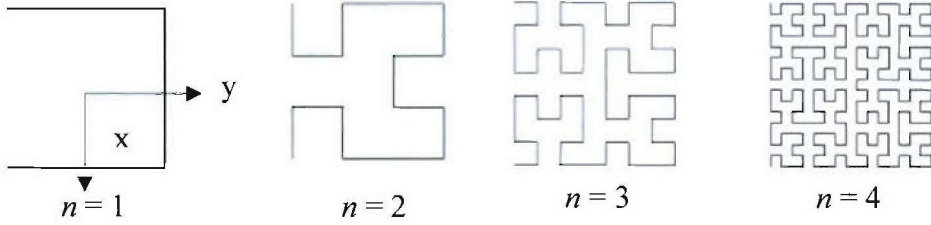$$d = L/(2^n - 1) ; S_h = (2^{2n} - 1)d = (2^n + 1)L \qquad (1)$$

Fig. 1: Geometry of Hilbert curves for the first four iterations. The plane $\phi = 0^0$ is the x-z plane.

Figure 2 shows the first four iteration orders of the Peano curves. For a Peano curve with side dimension L and order n, the length of each line segment d and the sum of all the line segments S_P are given by,

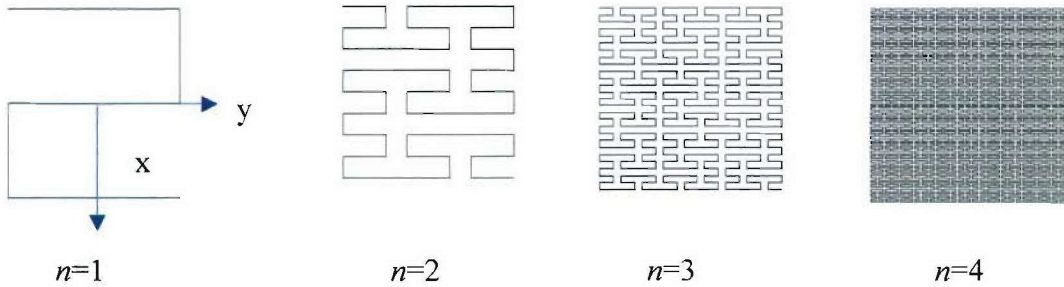$$d = L/(3^n - 1) ; S_p = (3^{2n} - 1)d = (3^n + 1)L \qquad (2)$$

Fig. 2: Geometry of Peano curves for the first four iterations. The plane $\phi = 0^0$ is the x-z plane

As can be seen, for a fixed area, the total length of the Hilbert or Peano curve increases as one increases iteration (step) order in an iterative filling of a 2 dimensional region. Planar structures, patterned after these SP-curves can offer a resonant structure that may have a very small footprint at low frequencies as the step-order, n, is increased. Also, it is evident from equations (1)-(2) and Figures 1 and 2 that the Peano algorithm has a higher compression rate in filling of a 2-D region than the Hilbert algorithm, thus, it could in

6

principle result in a structure with a lower resonant frequency than a corresponding Hilbert structure of identical footprint size and step-order. There are other SF-curves that one can consider for antenna applications; they include *Moore Curve, Lebesque Curve* and *Serpinski Curve* among many others [1]. In fact, the well-known *Fractals* are a subset of the space-filling curves.

In the following sections, we present the fundamental radiation characteristics of Hilbert and Peano antenna elements, mutual coupling between two such elements and potential use of these SF-curve elements in forming Yagi arrays for high gain applications.

2.1 *Hilbert Antennas*

As shown by others (see e.g., [2]-[5]), the Hilbert curve may provide an attractive solution for miniaturization of antennas. However, the questions naturally arise as to how a Hilbert antenna at its *fundamental* resonant frequency can be matched to a feed line with a given characteristic impedance (e.g., a 50-ohm line) and how the bandwidth and cross-polarization level of such a *matched* antenna may vary as one increases the iteration order, n,, in order to assess the suitability of such an antenna as a matched planar resonant antenna with an electrically small footprint. We have recently shown [6] that while a center-fed antenna may result in a very small radiation resistance, a properly chosen off-center feed point can always provide, regardless of how high n is, a 50 ohm match required for most applications. In general, for an antenna occupying a fixed square
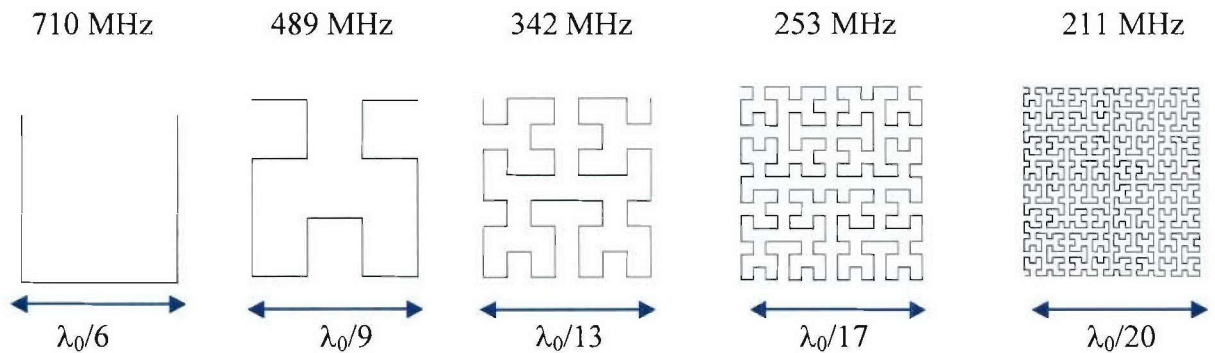
| 710 MHz | 489 MHz | 342 MHz | 253 MHz | 211 MHz |

| $\lambda_0/6$ | $\lambda_0/9$ | $\lambda_0/13$ | $\lambda_0/17$ | $\lambda_0/20$ |

Fig. 3: The resonant frequency and electrical dimensions of the matched Hilbert

surface area of L x L, increase of n from 1 to 5 drastically lowers the resonant frequency

by a factor of three or higher. This reduction in the resonant frequency, however, is achieved at the expense of a bandwidth that is very small when n=5. Figure 3 shows the resonant frequency and electrical dimensions of the first five iteration orders of Hilbert antennas, matched to a fifty ohms line when L=70mm. These results were obtained by using a method of moment (MOM) based numerical code. For the n=5 case, the antenna resonate at 219 MHz but has an electrical side dimension of only about 1/20 of wavelength, whereas its total length, when stretched along a straight line is about 1.63 wavelength. For comparison, a microstrip patch antenna with an air-substrate, and with an identical footprint, has a resonant frequency of more than 2GHz, albeit with a higher bandwidth. The input impedance and VSWR as a function of frequency together with the far-field

Figure 4: Input impedance, VSWR and Patterns of a Hilbert antenna of order 3.

patterns at resonance, are shown in Figure 4 for n=3 case. One interesting feature of the Hilbert antenna is that its pattern resembles that of a dipole. Similar pattern behaviors are also observed for other iteration orders. It is also noteworthy that Hilbert antenna is a multi-resonant structure [6].
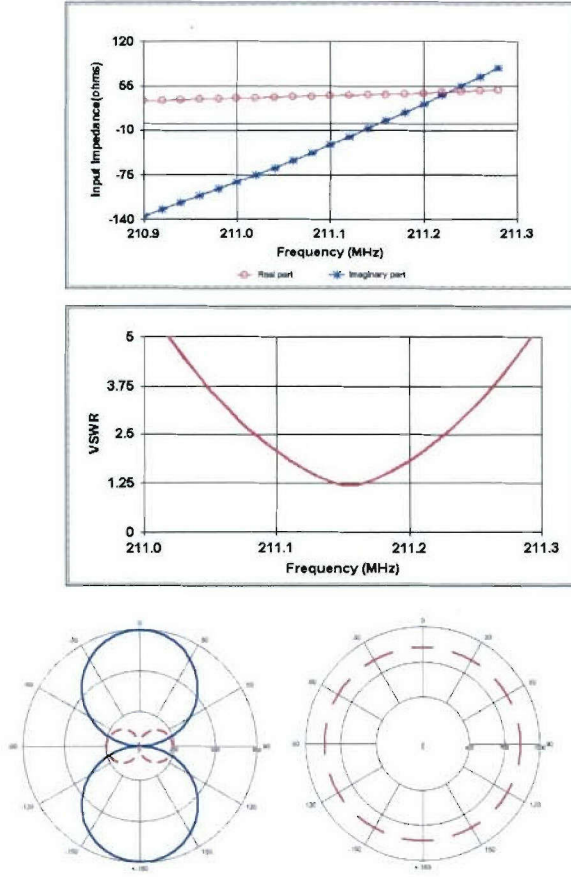
2.2 Peano Antennas

The matched Peano antennas were recently introduced by the PI and his co-authors in [7]. The preliminary results show that, just like the Hilbert antennas, these antennas can also be matched to a 50 ohm or 75 ohm line using a properly chosen off-center feed location, as shown in Figure 5. We notice that for n = 3, the outer dimension of the antenna is only

8

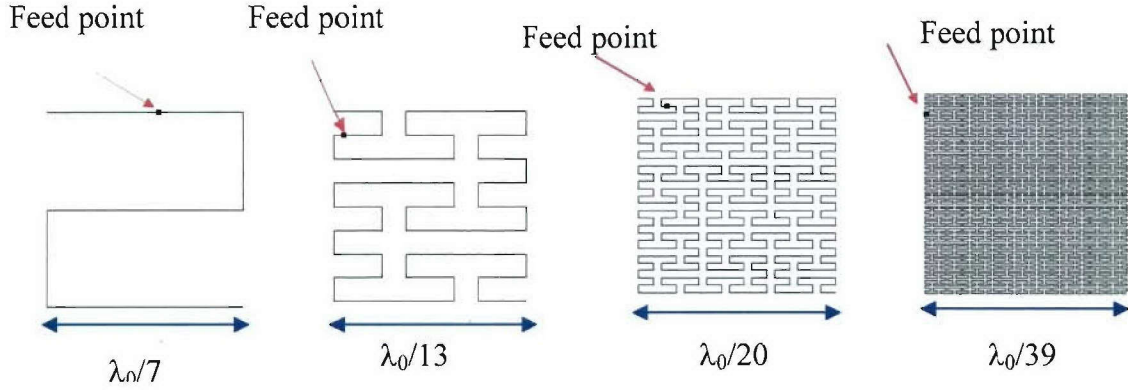about 1/20 of its first resonant wavelength, and the antenna is still matched to a 50-ohm

Fig. 5: The resonant frequency and electrical dimensions of the matched Peano antennas for the orders n = 1 to 4. All antennas are 70mm x 70 mm.

line at its fundamental resonance. While for the same order Hilbert antenna the outer dimension is about 1/13 of its first resonant wavelength. In general, for a given footprint and a fixed step order n, the Peano antenna has a longer total length, resonates at a lower fundamental resonant frequency and, therefore, results in an electrically more compact radiator than a comparable Hilbert antenna, albeit at the expense of a smaller input-impedance bandwidth as shown in Figure 6. This is expected because of the relatively higher compression rate of the Peano-curve algorithm in filling of a 2-D region. On the other hand, for a given resonance frequency, Peano antenna has nearly the same bandwidth as that of a Hilbert antenna; this is evident by comparing, for example,

Table 1. The cross-polarization for Peano antennas

n		1	2	3	4
Cross -Pol level (dB)	Phi=0	-11.8	-60.3	-57.2	-60.1
	Phi=90	-13.7	-60.3	-57.2	-60.1

Table 2. Radiation Efficiency (%) of Peano and Hilbert antennas

n	1	2	3	4	5
Hilbert Antenna	98.9	93.8	75.2	41.1	17.2
Peano Antenna	97.1	72.3	17.5	-	-

the Peano antenna of order n=2 with the Hilbert antenna of order n=3 in Figure 6. The Peano antenna, however, has the advantage of having a much lower cross-pol level than the Hilbert antenna, as shown in Table 1. As seen, except for the case of n=1, the Peano antennas have very low cross-pol levels (about −57 dB or lower) that are nearly identical in both $\phi=0^\circ$ and $\phi =90^\circ$ planes (see Figure 7) . This can be explained from the central

symmetric nature of the current distribution in the Peano antennas shown in Figure 8. For the Hilbert antennas, however, the cross-pol levels are much higher in the $\phi=90^{\circ}$, which can be attributed to the mirror-image symmetry of the current distribution [6].
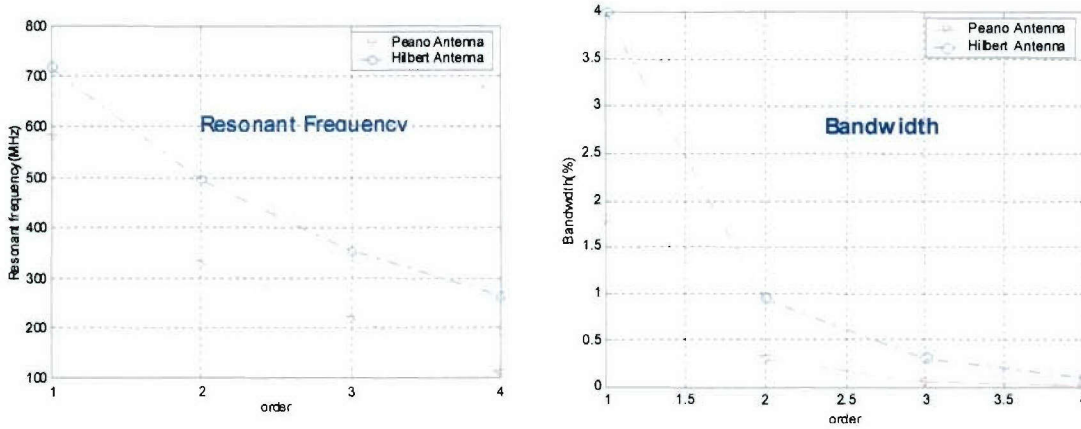

Fig. 6: Comparison of the resonance frequencies and bandwidths of Hilbert and Peano Antennas
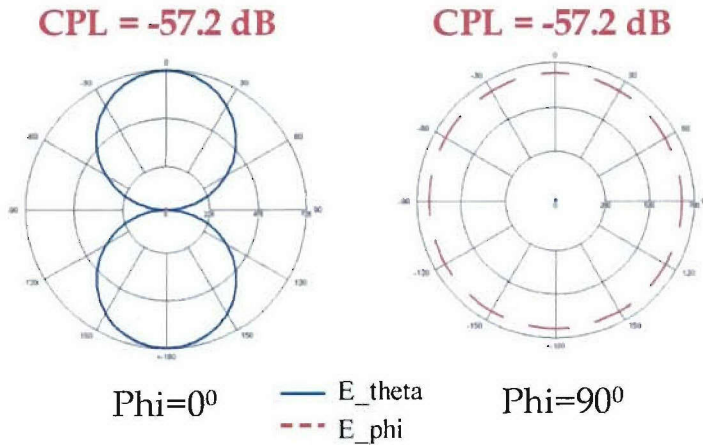

Fig. 7: Radiation patterns of the Peano antenna of order n = 3

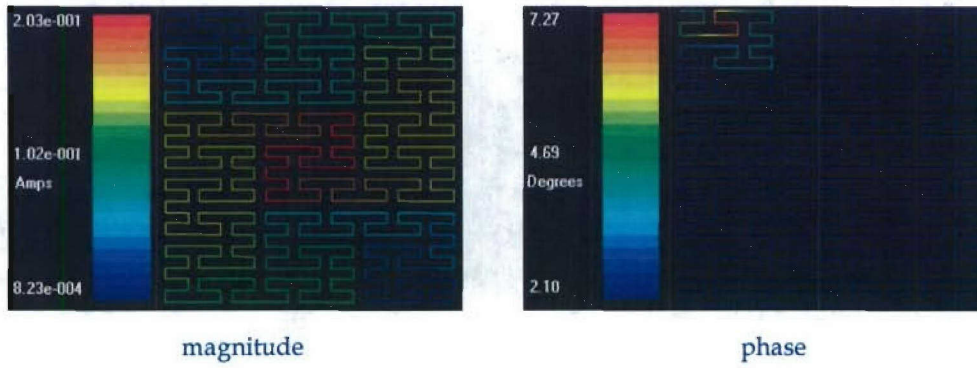magnitude   phase

Fig. 8: The current distribution on the 3rd order Peano antenna

Finally, a comparison of the radiation efficiency of the Hilbert and Peano antennas is shown in Table 2. In computing the radiation efficiency, both antennas are assumed to be made of copper. It should also be noted that, as in the case of Hilbert antenna, Peano antenna also exhibits multi-resonant behavior [7].

2.3 Experimental Results

In order to verify the characteristics of the space-filling curve antennas, we fabricated a printed second-order Peano antenna. The antenna is designed using a moment-method based simulation tool. The geometry of the antenna is shown in Figure 9. The dielectric constant of the substrate is 2.3 and the thickness is 0.5mm. Using the equivalent width ratio of w/a = 4 [8], the width of the copper strip is set to 2mm, since the radius of the wire we used in the simulations in the previous section was a = 0.5mm. The feed point is chosen to match a 50-ohm transmission line as before. The feed gap is 0.5mm as shown in Figure 9. The outer dimension of the antenna is 31mm x

Fig. 9. The geometry of the printed Peano antenna

31mm. The simulation shows that the first resonant frequency is 772.5MHz and the second resonance is 1.16GHz.

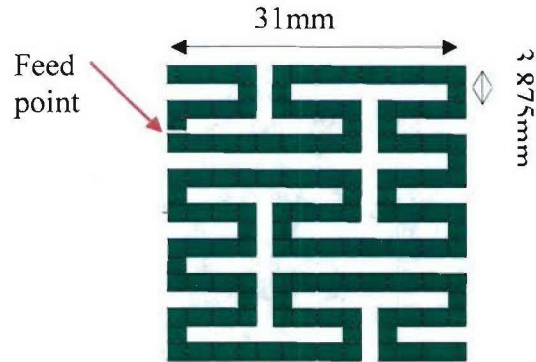The fabricated second-order Peano antenna together with the measured VSWR is shown

in Figure 10. The frequency sweep is from 500 MHz to 2.0 GHz (150 MHz per division) and the vertical scale is VSWR (1 per division). The best resonance is at 1.1 GHz (curser) with a VSWR of 1.36:1 and the bandwidth is ~60 MHz at 3.0:1 VSWR. We see that only the second resonant frequency, 1.1 GHz, which is very close to the simulation result, is observed.
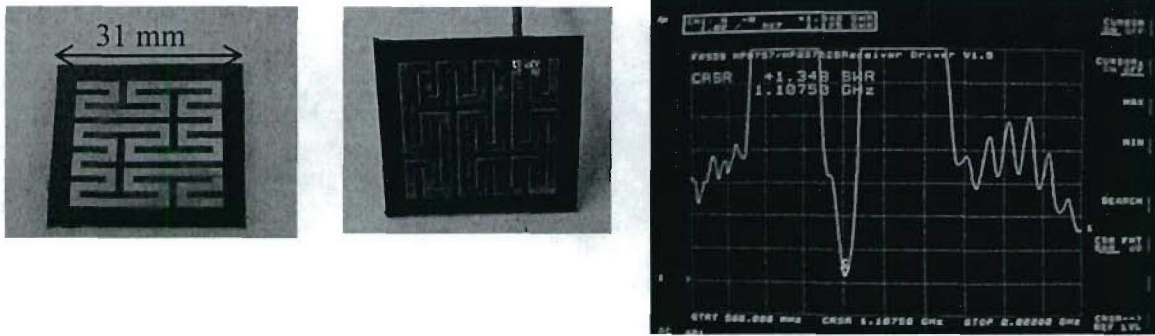

Fig. 10: Fabricated 2nd order Peano antenna and its measured VSWR.

The reason we did not capture the first resonance is that the antenna was designed to be fed with a 50-ohm co-strip line, but actually it is fed with 0.085" 50-ohm semi-rigid coax as can be seen in Figure 10. The coax is an unbalanced line and the current flowing on the feed cable radiates and interferes with the first resonance of the Peano antenna, so that the first resonance is not clearly observed. To avoid the unbalanced feed, an alternative feeding technique will be to use a co-strip line feed that connects to a grounded coaxial

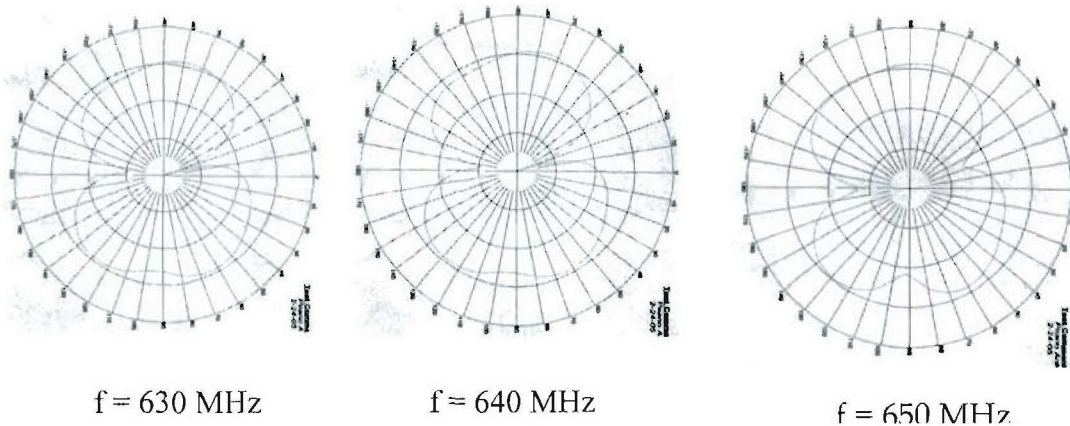f = 630 MHz   f = 640 MHz   f = 650 MHz

Fig. 11: Measured pattern of the 2nd order Peano antenna

cable at a distance away from the antenna feed point.

To observe the first resonance of the antenna in Figure 10 and measure its radiation pattern, we designed a Balun to balance the coaxial feed. A resonant frequency of about 640 MHz was observed. The corresponding normalized measured pattern is depicted in Figure 11. As it was theoretically predicted, the pattern is like that of a short dipole.

Alternative feeding techniques when the Peano or Hilbert antenna in fabricated on a substrate are shown in Figure 12. In one scheme, when the antenna is on substrate without a ground-plane, the antenna is fed either by a co-strip line, which is then transitioned to grounded coaxial line. In another scheme, when the antenna in fabricated on a grounded substrate, the antenna is fed by a microstrip line which is then transitioned to a coaxial line.
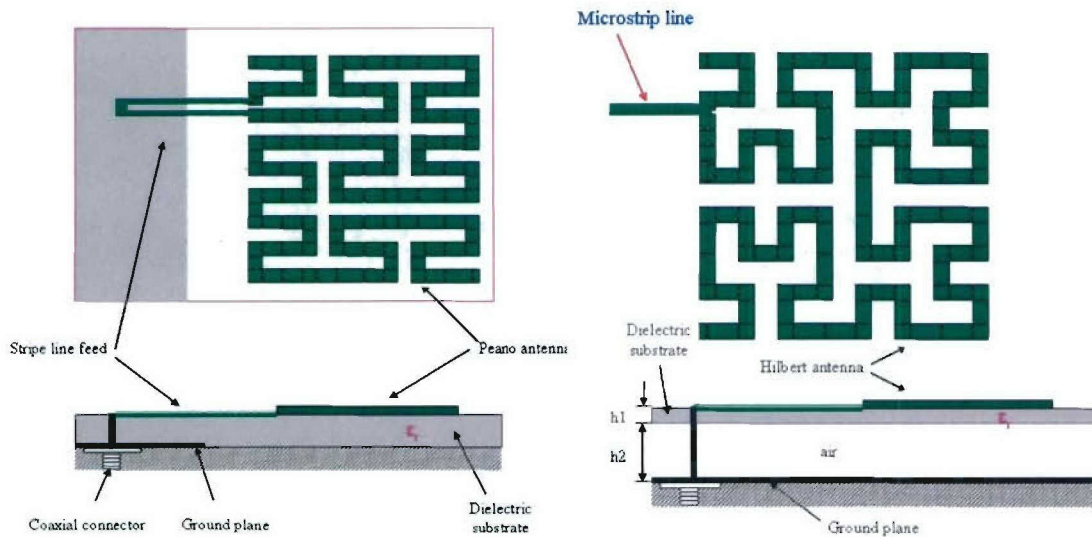

Figure 12: Feeding schemes for a Peano antenna without ground-plane (left), and a Hilbert antenna with a ground-plane (right).

3. Mutual Coupling Effects and Space-filling Curve Arrays

Hilbert and Peano antenna elements can be used to form compact collinear, two-dimensional or other specialized antenna arrays. Since these elements occupy electrically small areas they can be packed more densely than some other conventional planar antennas like patch or collinear printed dipoles. For high gain applications one may use these elements to develop Hilbert or Peano Yagi arrays, as shown in Figure 13. Another interesting application will be in reduction of co-site interference between radios operating in the same frequency band, which is a critical problem for some military applications. An antenna with narrow instantaneous bandwidth
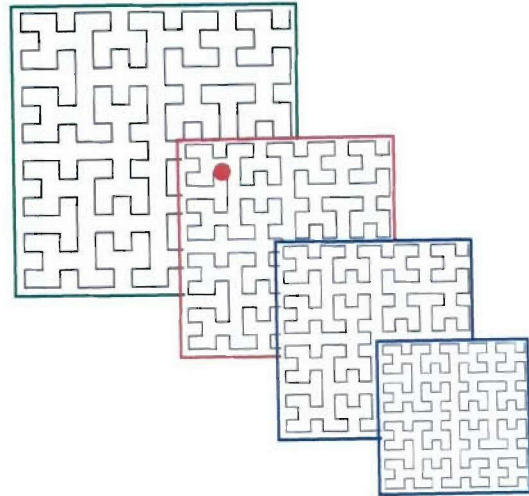

Fig. 13: A Yagi array of Peano antenna elements

can provide out of band rejection to unwanted signals. Acting much like RF bandpass filter the antenna can offer significant attenuation to out of band signals. Depending on the order and size, Peano and Hilbert antenna elements can provide extremely narrow instantaneous bandwidth. Key to utilizing this technology is developing a method to cover the full operating band of the radio by tuning this instantaneous band across the operating band or switching between elements tuned for specific portions of the operating band. For example, several of these SP-curve elements can be positioned next to each other or vertically stacked together to achieve the required multiband operation. Tuning and/or switching speeds would have to be compatible with modern frequency hopping radios.

3.1 Mutual Coupling Effects

The first step toward array designs will be to study the mutual coupling effects between a pair of Hilbert or a pair of Peano antenna elements in three different possible configurations, side-by-side, collinear and stacked.

In our calculation of coupling between two space-filling curve antennas, we have used the concept of "maximum coupling", which is computed using [9, 10]

$$C_{max} = \frac{1}{L_0}[1 - (1 - L_0^2)^{1/2}]$$ (3)

$$L_0 = \frac{|Y_{12}Y_{21}|}{2\,\mathrm{Re}(Y_{11})\,\mathrm{Re}(Y_{22}) - \mathrm{Re}(Y_{12}Y_{21})}$$ (4)

Where (Y11, Y22) and (Y12, Y21) are the self and mutual admittances of the two antennas, respectively.

Coupling between two Hilbert Antennas

Figure 14 shows the various arrangements for two Hilbert curve antennas. The maximum coupling for two third order Hilbert antenna in side-by-side, collinear and stack arrangements as a function of the element separation *s* is shown in Figure 15. We have
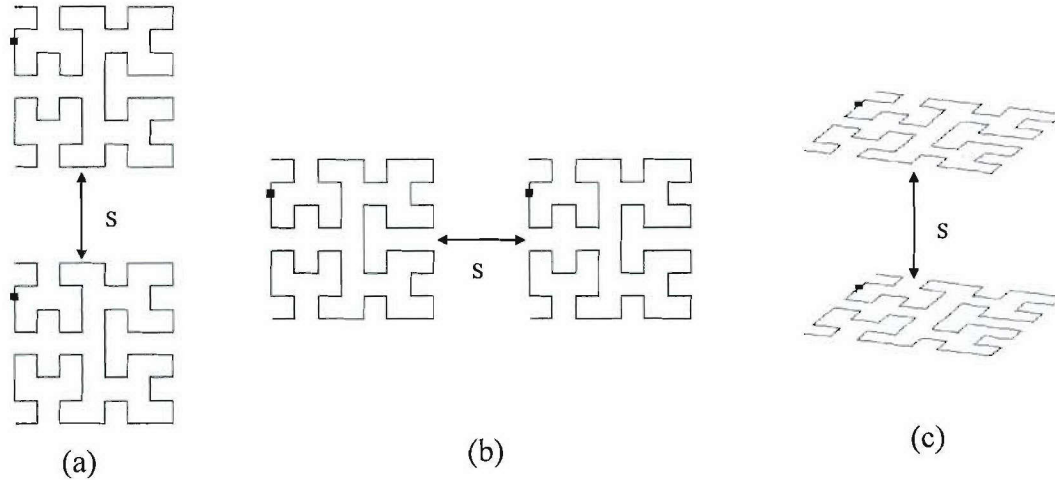

(a)   (b)   (c)

Fig. 14: Two identical Hilbert antennas in the following arrangements:
(a) collinear; (b) side-by-side; and (c) stacked

shown in previous section that the radiation patterns of the Hilbert antenna almost resemble the patterns of a linear dipole. Therefore, as expected, we see the couplings for side-by-side case and stack case are almost the same. At the same time, the side-by-side and stack arrangements exhibit much stronger coupling when the spacing is larger than about 0.3λ, since the elements are placed along the direction of their respective maximum

15

radiation.

We also have investigated the effect of proximity of two Hilbert antennas on matching of the fed antenna. Two 3rd order Hilbert antennas are positioned in three arrangements as before and only one is fed, as shown in Figure 14. We plot the $|S_{11}|^2$ to see the variation of matching in different separations: 0.1λ, 0.25λ and 0.5λ. The feed point is fixed at 50-ohm matching point for one antenna. The results are shown in Figure 16.
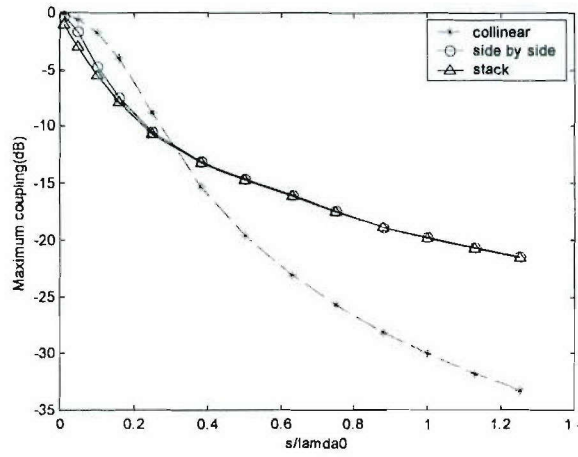

Figure 15: Maximum coupling for the two Hilbert antenna of order n=3 in side-by-side, collinear and stack arrangements as a function of the element separation.

Coupling between two Peano Antennas

The various arrangements of the two Peano antennas are shown in Figure 17. The results of maximum coupling as a function of the element separation s are shown in Figure 18. Just as in the case of the Hilbert antenna, the radiation patterns of the Peano antenna also resemble the patterns of a linear dipole. Therefore, the couplings for side-by-side and stack cases are almost the same. In this case, the side-by-side and stack arrangements exhibit much stronger coupling when the spacing is larger than about 0.33λ, which is slightly larger than that in the Hilbert case. When the spacing is less than 0.33λ the side-by-side and stack cases exhibit smaller coupling than the collinear case. However, for $s > 0.33\lambda$, the collinear arrangement exhibits smaller coupling. Finally, the coupling effect on the matching of a Peano antenna is also studied. Two 2nd order Peano antennas are positioned in three arrangements as before and only one is fed. The feed point is fixed at

16

50-ohm matching point for one of the two Peano antennas. The effects of separation distance, s, on the return loss are shown in Figure 19.
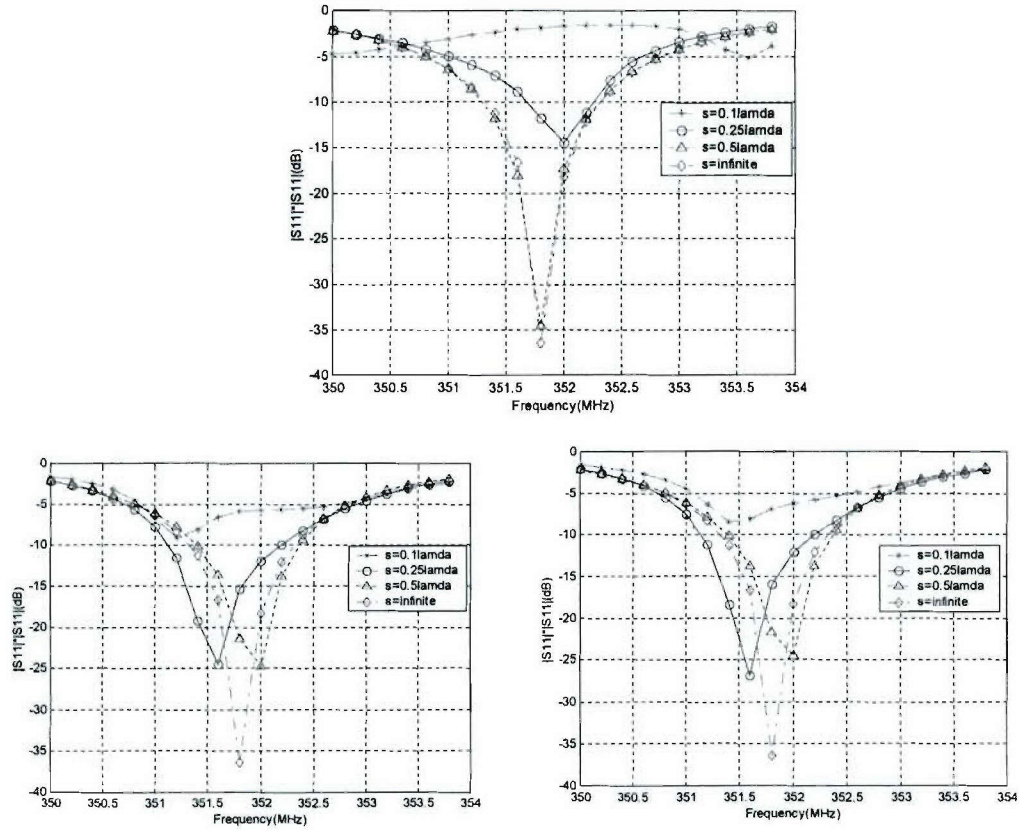

Figure 16: $|S_{11}|^2$ for two 3rd order Hilbert antennas shown in Figure 38 with different separations in three arrangements: (top). collinear; (left). side-by-side; (right). stack.
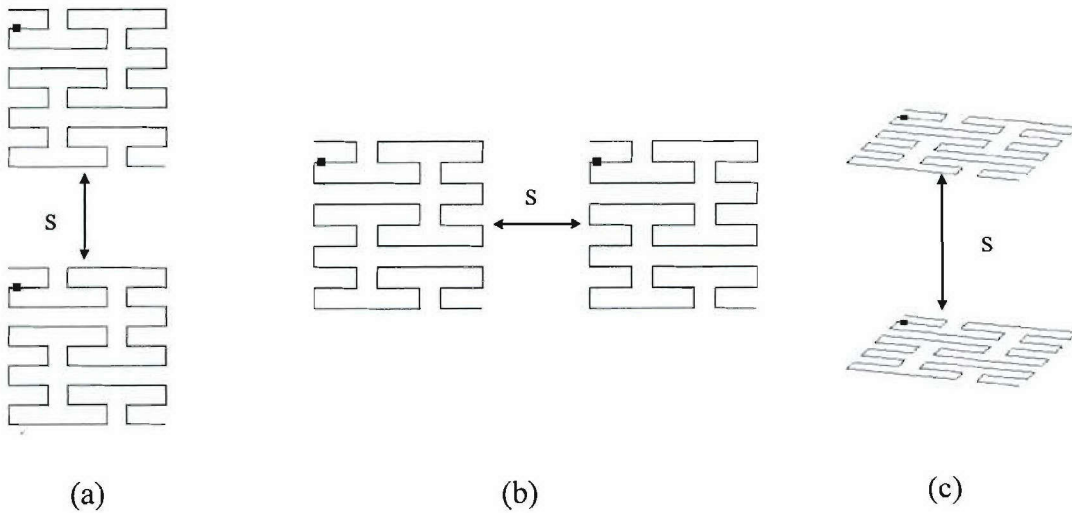

(a)   (b)   (c)

Fig. 17: Two identical Peano antennas in the following arrangements:
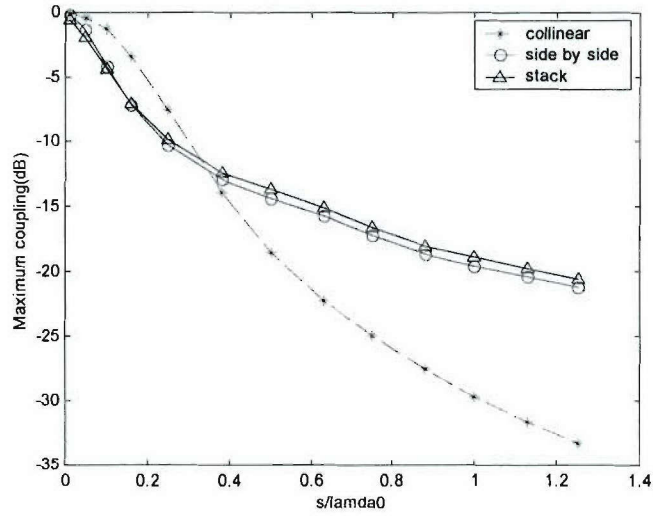(a) collinear; (b) side-by-side; and (c) stacked

17

Figure 18: Maximum coupling for the two 2nd order Peano antenna in side-by-side, collinear and stack arrangements as a function of the element separation.
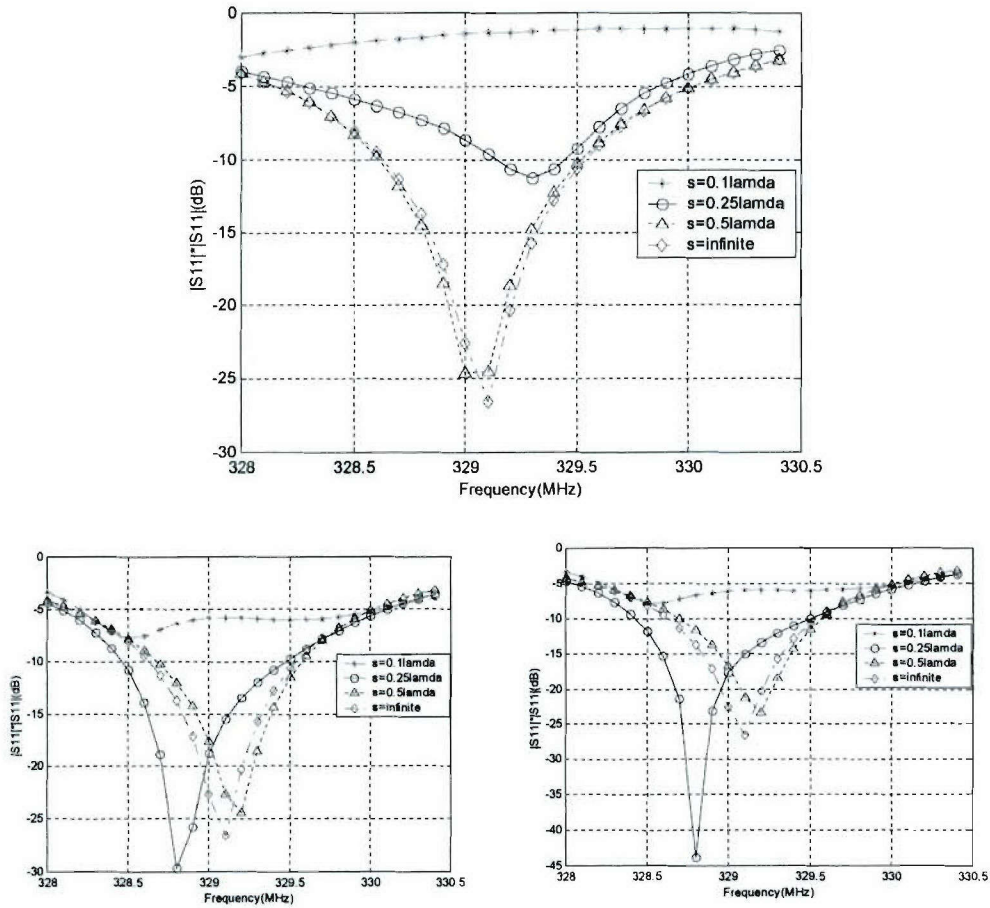

Figure 19: $|S_{11}|^2$ for two 2nd-order Peano antennas with different separations in three arrangements: (top). collinear; (left). side-by-side; (right). stack.

Comparison with λ/2 Dipole

Next, we compare the results of our coupling analysis for Hilbert and Peano antennas, with that of the mutual coupling for simple linear resonant λ/2 dipoles in collinear, side-by-side, and stacked configurations. The results are shown in Figure 20. Our results show that for these antennas the mutual coupling in the collinear configuration is higher than that of the simple resonant dipoles in the same configuration. For the side-by-side and stacked configurations, mutual coupling for these space-filling-curve antennas is somewhat similar to the case of resonant dipoles. However, these antennas occupy much smaller footprints, and thus they can be packed more densely in the collinear configuration.
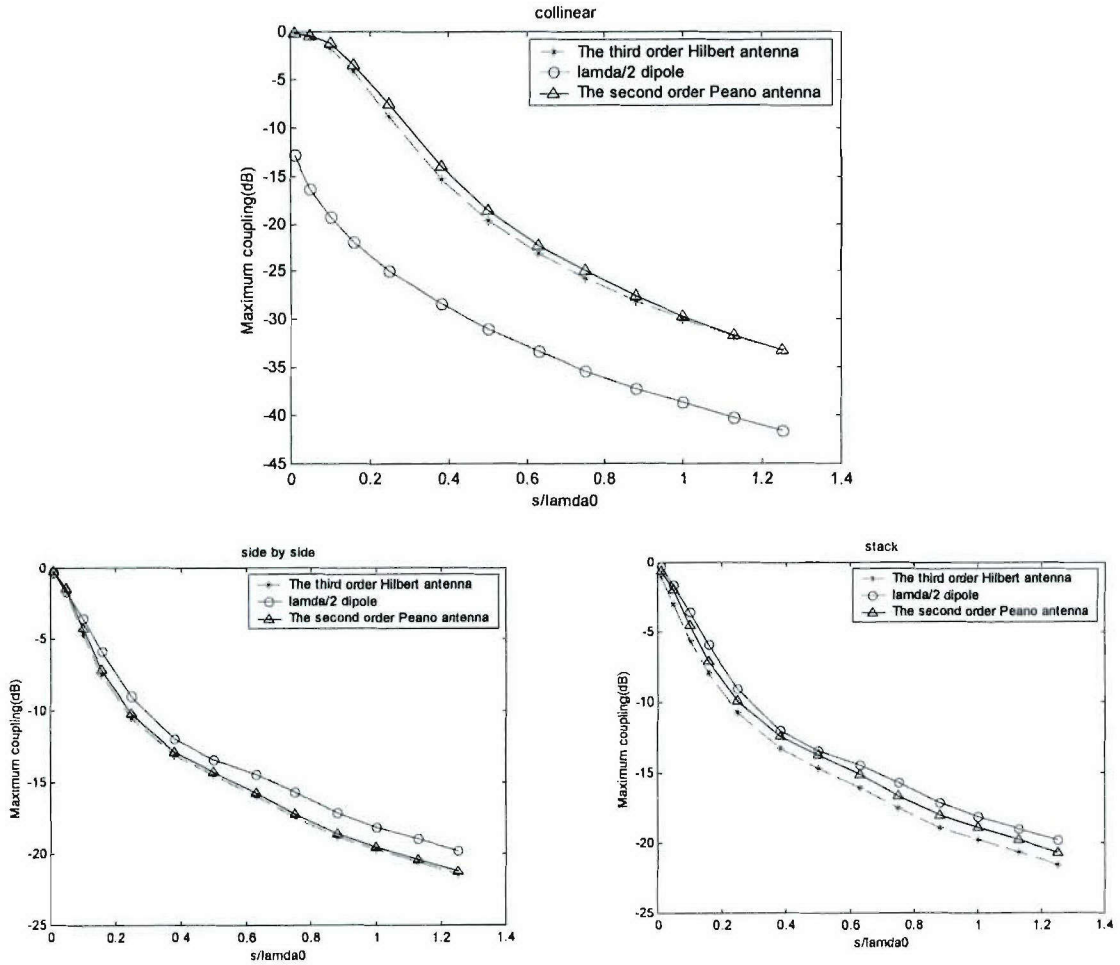

Figure 20: Comparison of maximum coupling between Hilbert antenna, λ/2 dipole and Peano antenna in three arrangements: (top). collinear; (bottom). side-by-side and stack.

3.2 SF-Curve Yagi Arrays

Various possible configurations of a Yagi array above a ground-plane made of space-filling curve elements are shown in Figure 21. In this section, we present some preliminary results obtained by optimizing the dimensions of SF-curve elements, i.e., the driver (fed element), the directors and the reflector, for maximum directivity. Both Yagi arrays with and without ground-plane are optimized for comparison; in the former case, the height of the array above ground-plane is also included as an optimization parameter. An Evolutionary Programming (EP) algorithm (22) for continuous parameter optimization coupled with the Method of Moment based Numerical Electromagnetic Code (NEC) is used for optimization. Two cases presented here are those corresponding to the array configurations designated as the layouts 1 and 2 in Figure 21.

Yagi Array of Hilbert-Curve Elements

Here we present the results for a 2nd order Hilbert Yagi array. The Yagi arrays of Peano-curve elements are presently under investigation and the results will be reported in future. For EP optimization of the array directivity, the element dimensions SL_i's were constraint between 0.06λ to 0.15λ, whereas spacing distances S_{ij}'s varied with the range from 0.05λ to 0.2λ. The feed point location on the second element (the feed element) was also optimized. If the ground was present, the height of the Yagi above the ground was let vary from 0.01λ to 0.1λ. The wire radii of the Hilbert-curve elements were set fixed to 0.3 mm. Table 3 shows the results for both without and with the ground-plane cases. For the latter, the table shows both optimized results where only directivity was optimized as well as when the realized gain was optimized, i.e., when the directivity was optimized subject the to a 50-ohm matched condition of VSWR =1 at the center frequency. In these results, FTBR designates the front-to-back ratio in the array power pattern. For all cases, the bandwidth was very small, about 2 MHz at the center frequency of 497MHz. The array, however, has a much footprint of a comparable Yagi-Uda array of thin-wire half-wave dipoles or microstrip patch elements. If a four-element 2nd order Hilbert Ygai is configured like the layout 1 with ground-plane, for the best directivity, the volume of the optimal structure is $0.91\lambda*0.182 \lambda*0.078\lambda=0.0129*\lambda^3$. This volume can further be

decreased by using Hilbert-curves of higher orders.

The patterns and VSWR plots of the array for two cases in Table 1 are shown in Figures 22 and 23.
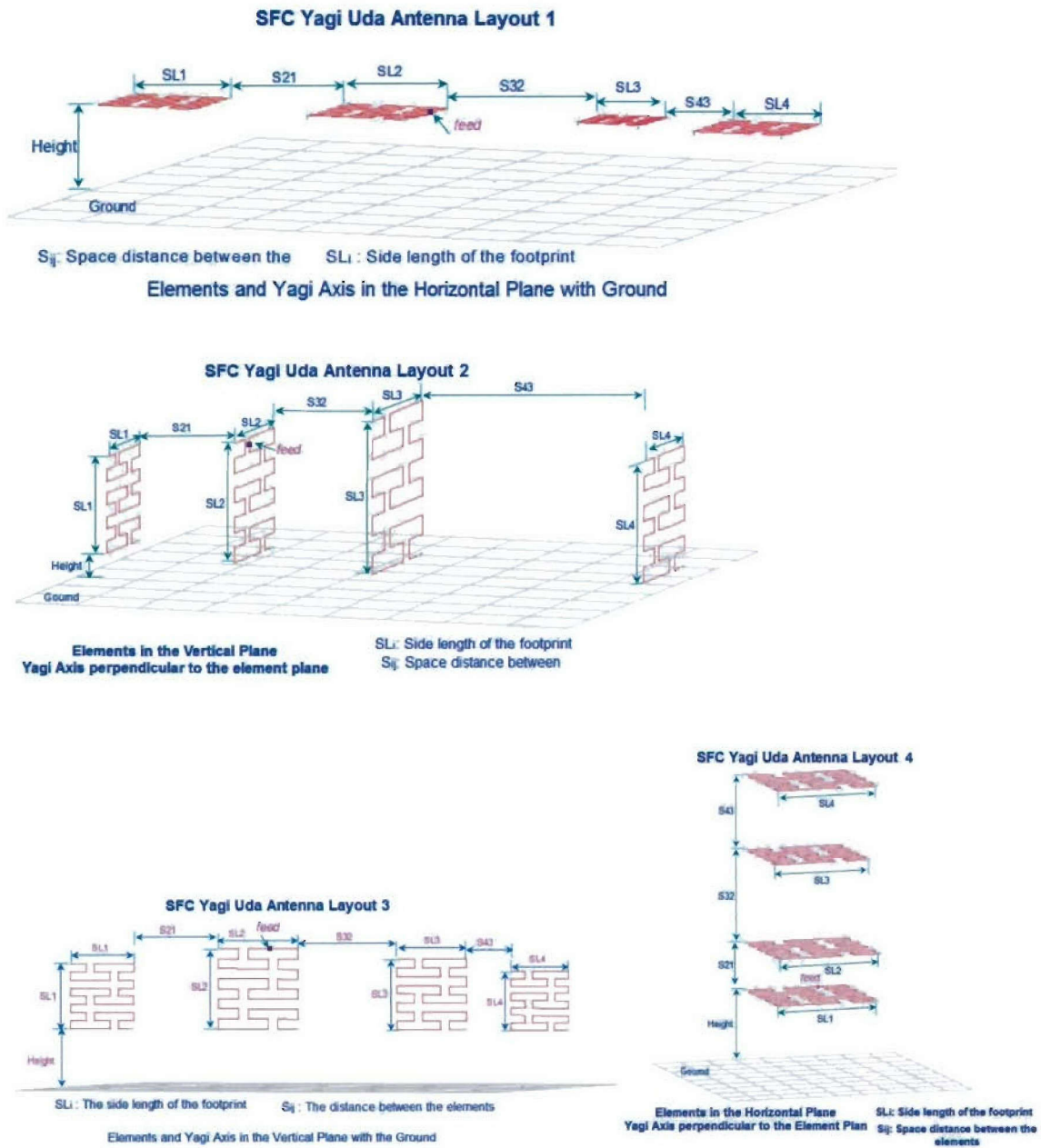

Figure 21: Possible configuration of SF-curve Yagi Arrays

Table 3: Four-element Yagi with 2nd Order Hilbert Antenna, Layout 1

H2Y4	Without Ground		With Ground	
	Directivity Optimization		Directivity Optimization	Gain Optimization
Feed Point	W: 18 S: 2		W: 30 S: 2	W: 30 S: 4
SL_1 (λ)	0.114		0.133	0.07
SL_2 (λ)	0.114		0.114	0.114
SL_3 (λ)	0.112		0.114	0.06
SL_4 (λ)	0.101		0.116	0.114
S_{21} (λ)	0.2		0.182	0.195
S_{32} (λ)	0.067		0.2	0.05
S_{43} (λ)	0.108		0.05	0.156
Height (λ)			0.078	0.096
Directivity (dBi)	7.14		9.34	9.1
VSWR	3.6		2.3	1.01
Realized Gain(dBi)	5.47		8.6	9.1
FTBR (dB)	10.97		*	*
Input Impedance (Ω)	13.7+j2.5		21.9+j8.65	50.4+j0.87
3dB Beam width (°)	110		70	70

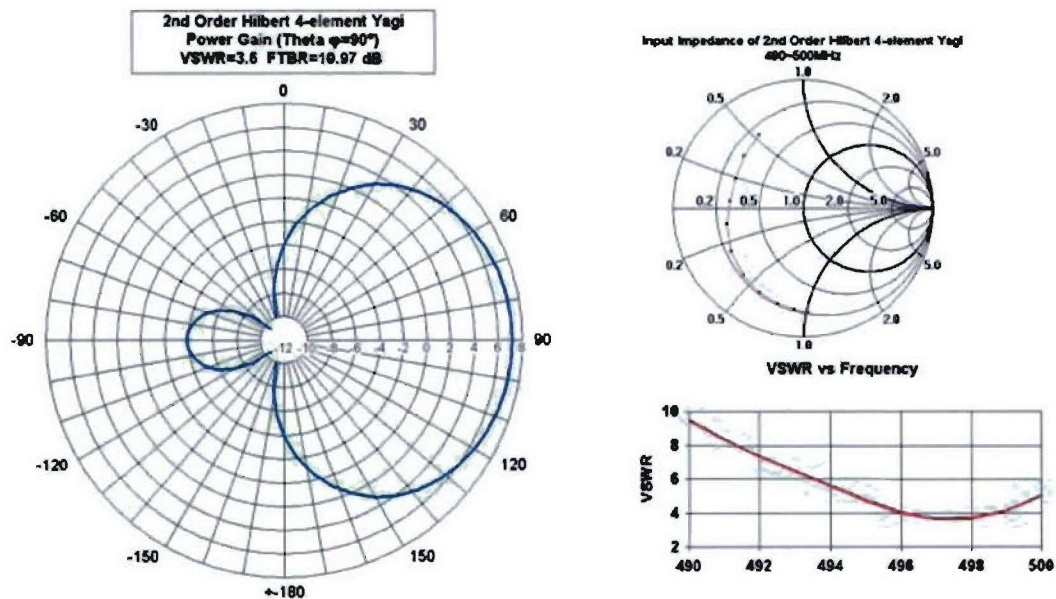The elements and the Yagi axis are in the same horizontal plane. 8 segments each wire.

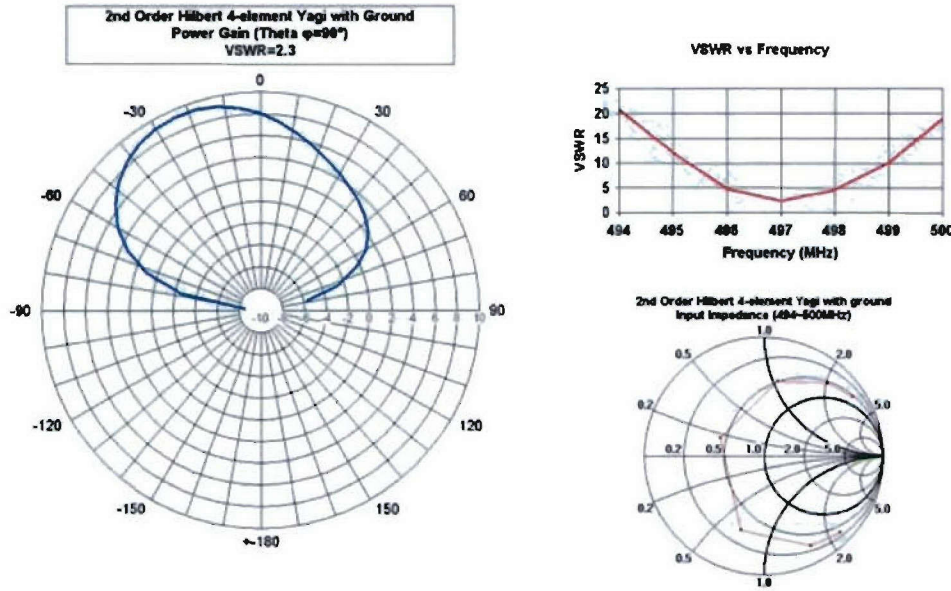Fig. 22: Pattern and VSWR of the 2nd order Hilbert Yagi array in free-space

Fig. 23: Pattern and VSWR of the 2nd order Hilbert Yagi array above a ground-plane

When the 2nd order Hilbert elements were placed in the vertical plane perpendicular to the Yagi axis (the layout 2 in the Fig. 21), the best directivity obtained was more than 8 dBi for non-grounded configuration, or greater than 12 dBi for the grounded version with satisfactory match (see Table 4). The total array length of the layout 2, for the maximal directivity configuration, is 0.507λ. The 50-ohm match constraint, however, did not result in a satisfactory realized gain where a gain of only about 5.22 dBi was obtained. This is mainly due to the poor front-to-back ratio (FTBR) of the optimized result, indicating any future optimization of these SF-curve arrays should perhaps include a constraint on a minimum FTBR value. Figures 24 and 25 show the pattern and VSWR characteristics of the 2 cases given in Table 4.

23

Table 4: Four-element Yagi with 2nd Order Hilbert Antenna, Layout 2

| The elements are in the vertical plane and perpendicular to the Yagi axis. 8 Segments each wire.			
H2Y4	Without Ground	With Ground	
	Directivity Optimization	Directivity Optimization	Match Optimization
Feed Point	W: 30 S: 3	W: 17 S: 2	W: 17 S: 8
SL_1 (λ)	0.114	0.114	0.147
SL_2 (λ)	0.114	0.113	0.111
SL_3 (λ)	0.141	0.113	0.08
SL_4 (λ)	0.113	0.1125	0.101
S_{21} (λ)	0.163	0.198	0.168
S_{32} (λ)	0.178	0.193	0.05
S_{43} (λ)	0.145	0.116	0.144
Height (λ)		0.065	0.01
Directivity (dBi)	8.35	12.67	5.22
VSWR	2.1	1.4	1.004
Realized Gain(dBi)	7.85	12.55	5.22
FTBR (dB)	8.79	8.8	0
Input Impedance (Ω)	51.4+j37	37.1+j7.18	50+j0.152
3dB Beam width (°)	60	30 (Half Beam)	45 (Half Beam)
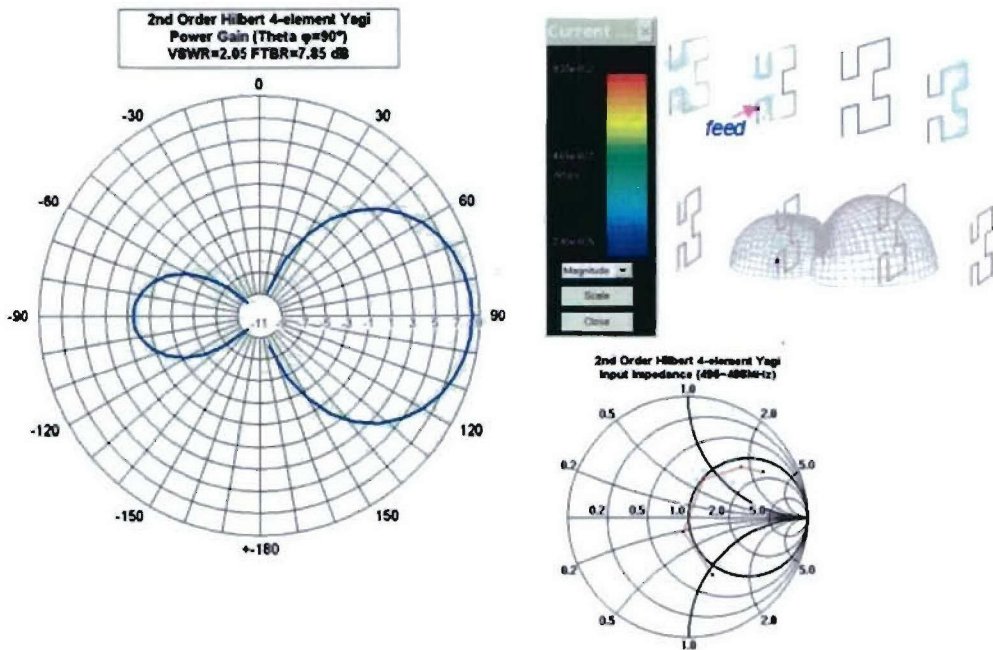
Fig. 24: Pattern and VSWR of the 2nd order Hilbert Yagi array without a ground-plane
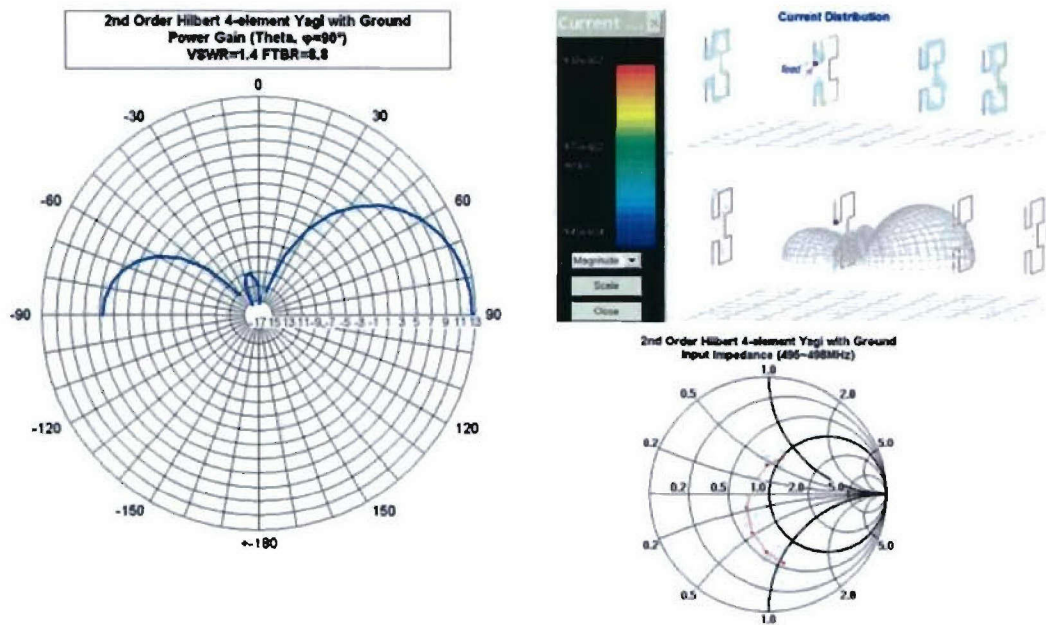
24

Fig. 25: Pattern and VSWR of the 2nd order Hilbert Yagi array above a ground-plane

4. Hilbert and Peano High Impedance Surfaces

High impedance surfaces (High-Z), also known as artificial magnetic conductors (AMC), have received considerable attention in the last few years [11-16]. These surfaces have a reflection coefficient of Γ=+1, when illuminated with a parallel-polarized plane wave, instead of the typical Γ=-1 for a conventional perfectly electric conducting (PEC) surface. These structures can obviously offer interesting applications in the antenna design [11-15] and for thin absorbing screens [16]. For example, a dipole antenna above such a metamaterial surface will have an image current with the same phase as the current on the dipole, resulting in an enhanced radiation performance. Several different types of high-impedance ground planes have been studied by various research groups (see e.g., [11-14]).

Previously we have shown that a metamaterial surface constructed with 2-D periodic arrangement of Hilbert curve inclusions above a conducting ground plane can act as a high impedance surface within a certain frequency band, providing a reflection coefficient of magnitude 1 with a phase angle of 0° [17]. The frequency at which this surface becomes a high-impedance surface is primarily related to the order number of the Hilbert curve (i.e. the length of the curve). The geometry of a Hi-Z surface using the Hilbert curve of order n=3 together with the corresponding reflection coefficient as a
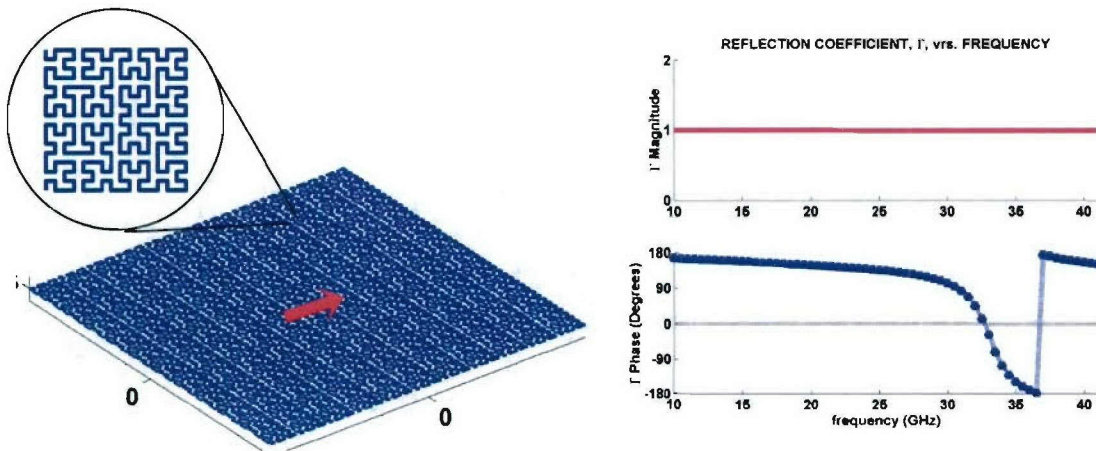

Fig. 26: A short dipole antenna over a Hilbert-curve Hi-Z surface, and the numerically predicted reflection coefficient when the surface is illuminated with a normally incident plane-wave. Note that the phase of the reflection coefficient has a zero degree transition region.

function of frequency is shown in Figure 26. Such SF-curve surfaces can have potential applications in enhancing the radiation of electrically small antennas [18], as shown in Figure 27, as well as possibly in bandwidth enhancement of planar antennas. In addition, for circular-polarized applications like GPS, when an antenna is located on or above a horizontal conducting surface, the horizontal polarized component of the circular polarization goes to zero at low angles. This results in the receive polarization essentially being vertical at low look angles, thus leading to a 3 dB reduction in received signal. Metamaterials Hi-Z ground planes offer the potential of improving the axial ratio at the GPS frequencies and thus resulting in improved gain at low look angles.
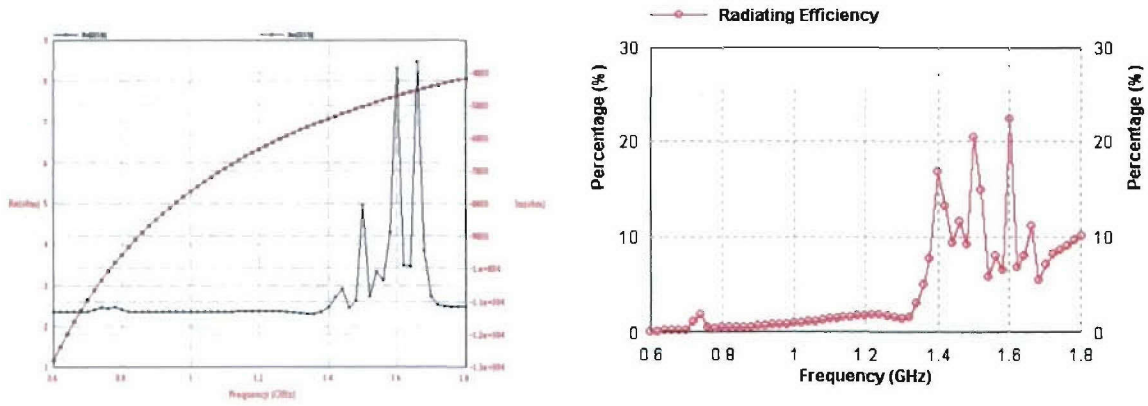

Fig. 27: Enhanced impedance properties (red: imaginary part; black: real part) of a short dipole antenna over a Hilbert-curve Hi-Z surface, and (right) the corresponding enhanced impedance radiation efficiency. Note that the efficiency is significantly increased near the frequency of operation of Hi-Z surface. Both the dipole and the surface are assumed to be made of copper.

In this section, we present further numerical and experimental results obtained during the course of the grant on use of Hilbert and Peano-curve inclusions to form High-Z surfaces, their applications on development of electrically thin absorbers for RCS reduction, and possible techniques to reduce polarization dependency of such surfaces.

4.1 Experimental Verification of a Hi-Z Hilbert Surface

A Hilbert surface of order 3 was constructed on an FR-4 epoxy (εr = 4.4, $\tan\delta$ = 0.02) substrate with a thickness of 1.575 mm. The Hilbert curve inclusions were scaled to a 12 mm x 12 mm footprint such that the resonance frequency, with the dielectric effects

included would fall within the range of the WR-430 waveguide (1.7-2.6 GHz) where the measurement is performed (see Figure 28). For Comparison, the waveguide and the Hilbert surface, including substrate losses were also modeled using Finite Element Method (FEM).

Figure 29 shows the reflection coefficient, magnitude and phase for the Hilbert surface at a height of 1.575 mm above the conducting ground-plane. When the phase passes through zero degrees, the surface has achieved resonance, the surface behaves as a Hi-Z surface (AMC), and the losses due to the FR-4 substrate are maximized. For this case, the total thickness of the AMC surface is just 0.01λ. As can be seen, very good agreement is obtained between the measured and the simulated results.
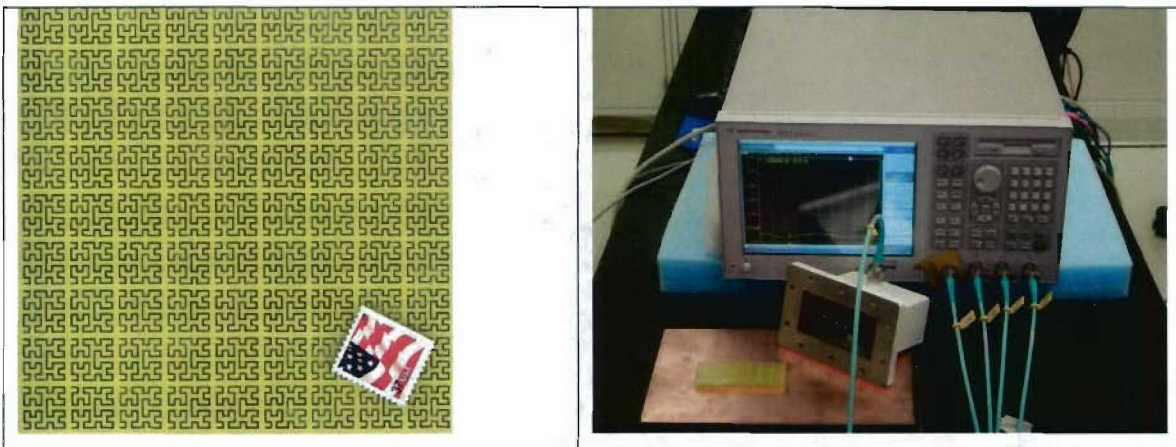

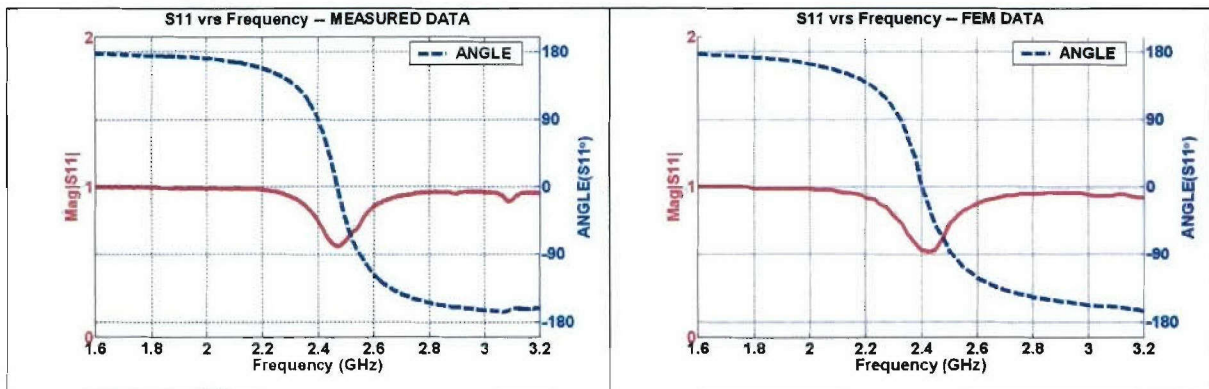Figure 28: Fabricated Hilbert Surface on FR-4 Substrate and Measurement Set-up

Figure 29: S11 Measured (left) and Simulated Results (right)

4.2 Peano Curve High Impedance Surface

The Peano curve, orders 1 through 3 is shown in Figure 30. Surfaces created by a 2-dimensional periodic arrangement of these inclusions, as shown in Fig. 31, posses AMC properties when backed by, and placed within close proximity to a conductive ground plane [19]. As shown in the geometry of Fig. 31, when each Peano of order 2 inclusion is contained within a 30mm x 30mm footprint, and the 2-dimensional planer array of

Figure 30: Peano Curve Orders 1-3
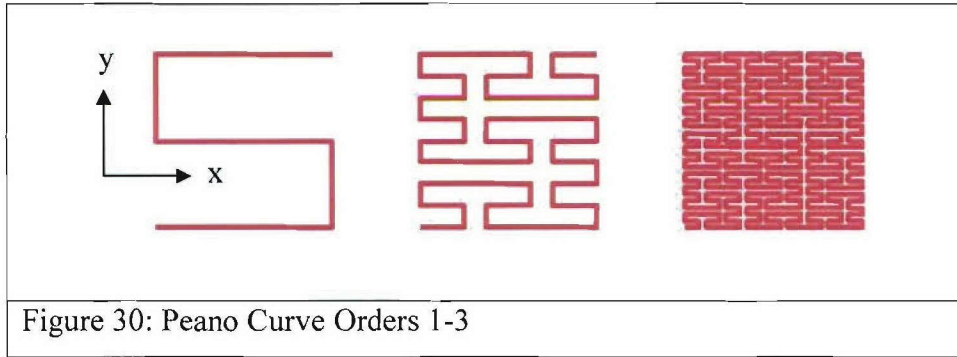
infinite extent is placed a distance of 15 mm above the conductive ground plane, the surface, illuminated by a normally incident plane wave, the surface gives rise to the reflection coefficient as shown in Figure 32, as a function of frequency.

Since the ground plane backing is of infinite extent, the magnitude of the reflection coefficient is always unity. The phase of the reflection coefficient however is shown have a transition through 0 degrees, at which point the surface is behaving as an Artificial Magnetic Conductor. The two curves correspond to

Figure 31: Peano Curve Surface of Order 2
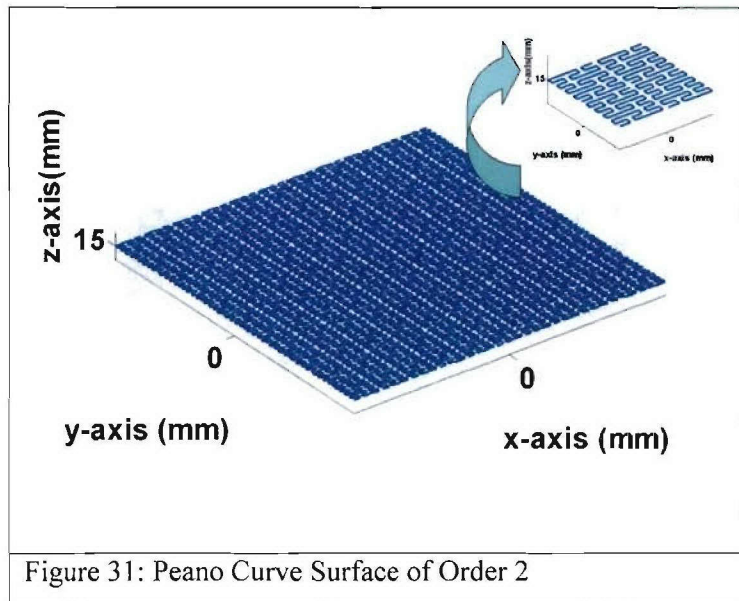
the two different and orthogonal polarizations studied and highlight the dependence that the resonant frequency has on the polarization of the illuminating electric field. As

indicated in Figure 32, for the x-directed electric field, the 30 mm x 30 mm dimensions which enclose each element in the surface is on the order of 0.15λ where λ is the wavelength at the frequency where the zero degree phase transition occurs. This highlights the fact that the inclusions are relatively small with respect to the resonant wavelength and that the distance between the periodic array surface and the ground plane is also electrically very small. For the y-directed polarization case, since the resonance occurs at a lower frequency, the
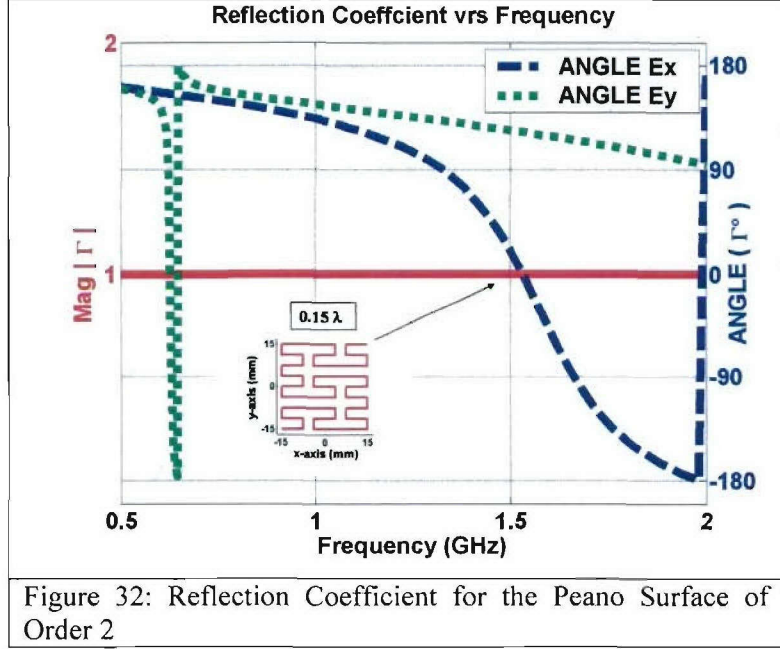

Figure 32: Reflection Coefficient for the Peano Surface of Order 2

dimensions are even smaller with respect to this wavelength and the bandwidth around the zero degree phase transition is also reduced, as would be expected.

We note that similar polarization dependency also exits for the Hilbert surface as has been reported in [17].

4.3 Polarization-Independent SF-Curve Surfaces

In this section, we address techniques for reducing and possibly eliminating the polarization dependence of AMC surfaces comprised of the space-filling curve inclusions. One potential solution to eliminate the polarization dependence is to create sub-arrays consisting of multiple inclusions rotated 90° with respect to one another. In this manner, these surfaces may have multiple resonances, independent of the polarization of the excitation.

Peano Surface

As an illustration, Figure 33 shows a polarization independent unit cell consisting of Peano curve inclusions, of order 2, utilizing this technique. A periodic boundary Method
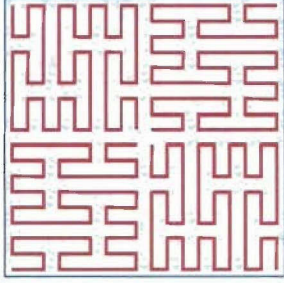

Figure 33: Dual-Polarized Peano Curve Sub-Array Element of Order 2
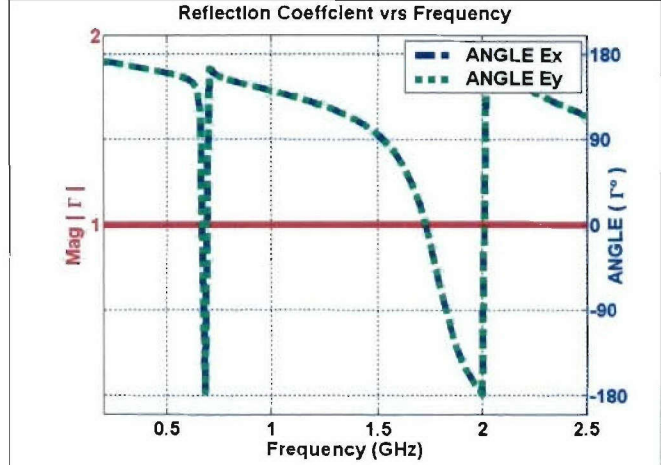

Figure 34: Reflection Coefficient for the Dual-Polarized Peano Curve Surface of Order 2

of Moments code is utilized, and the periodic boundaries are shown in Figure 33 with the blue line inclosing the sub-array. The magnitude and phase of the reflection coefficient for this periodic array of infinite extent, for the x-polarized and y-polarized excitations are shown in Figure 34. As can be seen the reflection coefficient, both magnitude and phase is completely independent of the polarization of excitation. Both resonances still occur; however, both resonances now occur no matter what polarization is used to excite the surface. The overall size of the sub-array is obviously now larger with respect to the resonant wavelengths, approximately twice the size, however since the individual inclusions are electrically small to begin with, the increase in size may be considered acceptable, depending upon the application considered. Using higher order curves would decrease the resonant frequency and thus reduce the overall size of the sub-array with respect to the resonant wavelength, however a reduction in the bandwidth would also occur.

Hilbert Surface

In a similar fashion, the dual-polarized/polarization independent Hilbert AMC surface can be analogously constructed. The sub-array (unit cell), and the reflection coefficient,

magnitude and phase, of the corresponding periodic array of infinite extent, are shown in Figures 35 and 36 respectively.
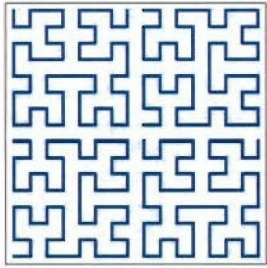

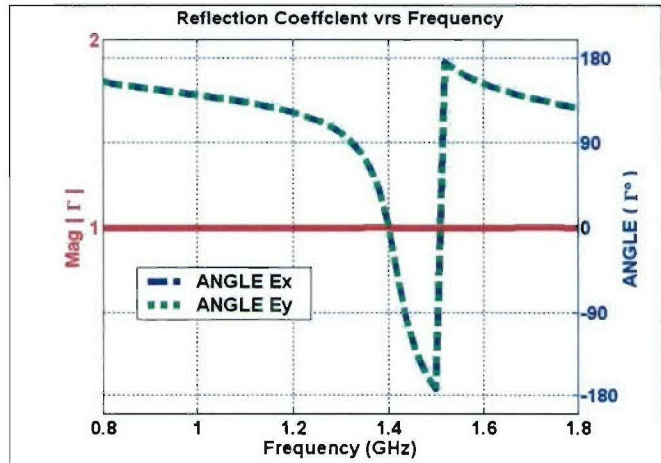Figure 35: Dual-Polarized Hilbert Curve Sub-Array Element of Order 3

Figure 36: Reflection Coefficient for the Dual-Polarized Hilbert Curve Surface of Order 3

4.4 Thin Absorbers Using Space-Filling Curve High Impedance Surfaces

In this work, artificial magnetic conducting ground-planes (AMC), created using a periodic arrangement of space-filling curves, are studied with respect to their use as an electromagnetic energy absorber. Two different surfaces are studied, corresponding to surfaces comprised of Peano curve inclusions of order 2 and Hilbert curve inclusions of order 3. The substrate effects of these surfaces are numerically studied using a periodic method of moment's code with an emphasis on substrate losses in the region where the surfaces behave as an AMC. To confirm the theory, measurements have also been performed with respect to the Radar Cross Section (RCS) of a metallic plate.

In a traditional single-screen Salisbury shield [20] a resistive layer is placed at a height of $\lambda/4$ above the conductor. This distance is not arbitrary and is, in fact, chosen due to the fact that the sum of the incident electric field and the reflected electric field reach a
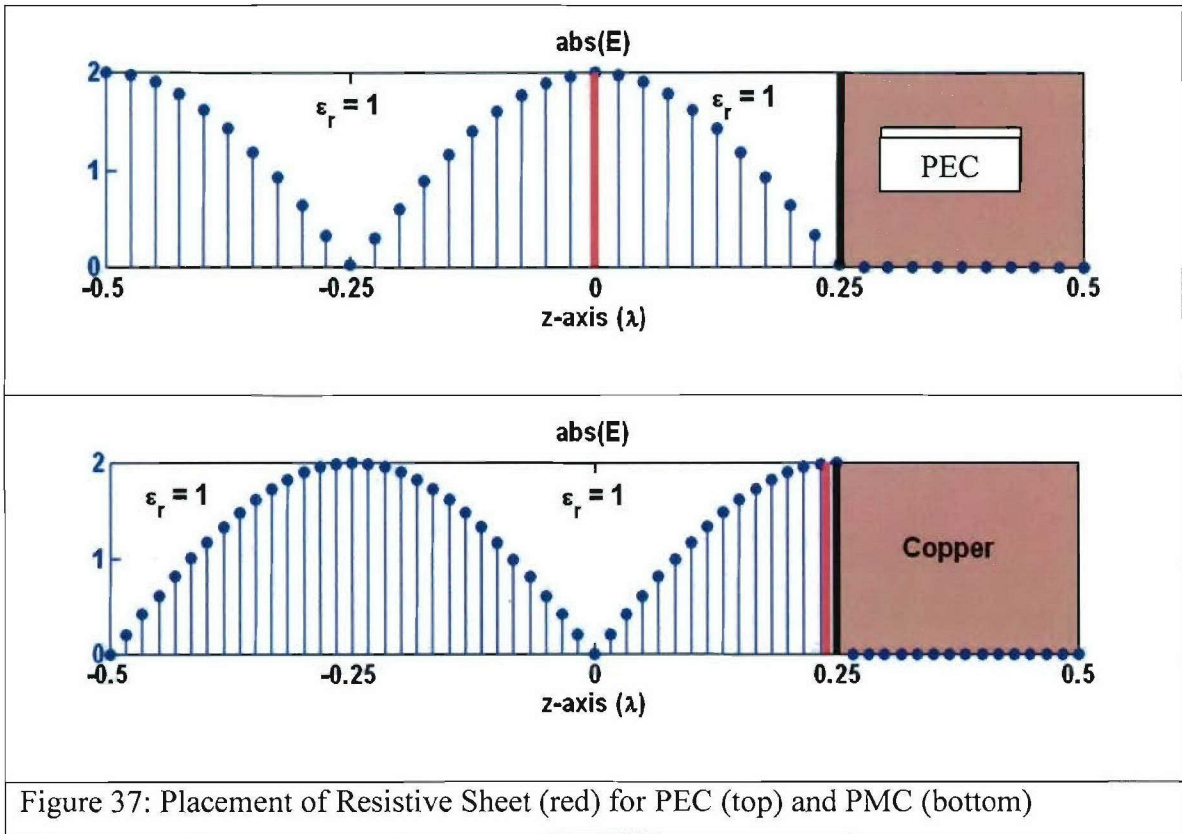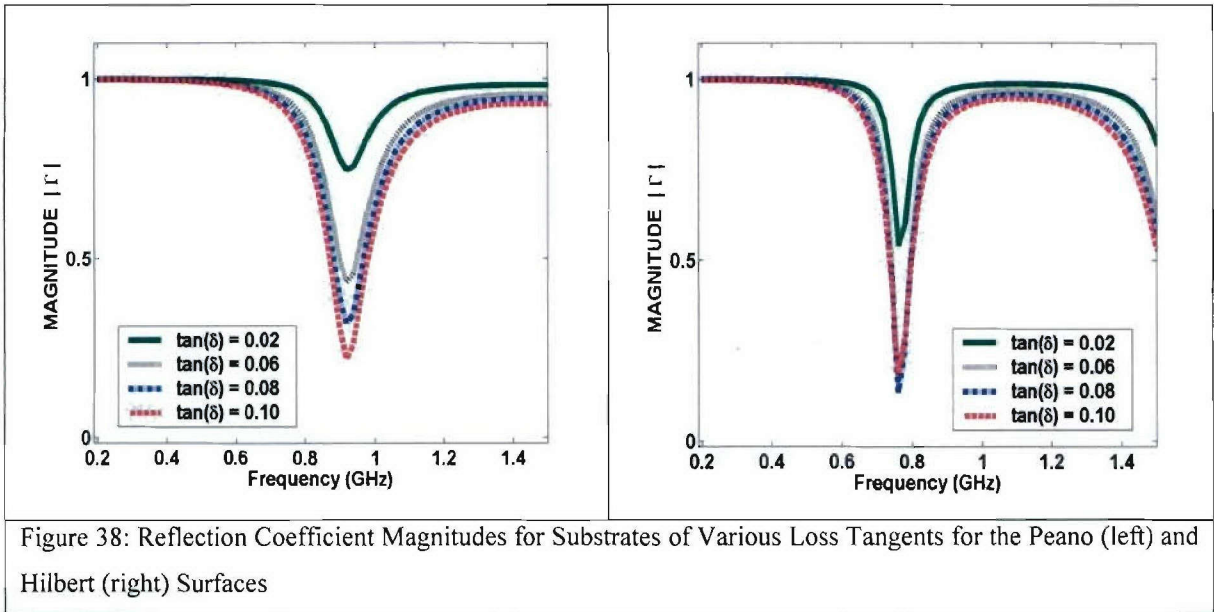

Figure 37: Placement of Resistive Sheet (red) for PEC (top) and PMC (bottom)

maximum at this distance (see Figure 37 (top)). By placing the resistive sheet where the electric field is maximum, the losses are thus maximized and the reflected energy is minimized, however this required distance of λ/4 limits the potential applications of this technique since this thickness is not always desirable. Another important issue arises concerning this distance, namely bandwidth, since the λ/4 distance is only achieved for a single wavelength.

It has been shown previously that a general artificial magnetic conductor (AMC) can be used to design a thin absorber [16], with thickness far less than the standard Salisbury screen. The basis is depicted in Figure 37 (bottom) where the incident and reflected electric field is shown when incident on a Perfect Magnetic Conductor (PMC) boundary. Since the tangential electric field is maximum at the interface with the PMC, the ideal location for the resistive sheet is at the PMC interface, thus providing absorbing properties in a low-profile and conformal geometry. Here we specifically study the Peano and Hilbert AMC's in this application.

Effects of the Loss Tangent

In numerical studies, substrate effects were added with the loss tangent of the material being the major focus. Figure 38 shows how the loss tangent of a 15 mm thick substrate

Figure 38: Reflection Coefficient Magnitudes for Substrates of Various Loss Tangents for the Peano (left) and Hilbert (right) Surfaces

affects the magnitude of the reflection coefficient for the x-polarized incident field case, as the loss tangent is varied from 0.02 to 0.10. For this numerical analysis, the footprint of the inclusions is again 30 mm x 30 mm and the height is 15 mm, corresponding to the free space numerical studies previously studied, as opposed to the fabricated dimensions presented above. A shift in the resonant frequency, as compared to the air-dielectric cases, is noticed, due to the real permittivity of the material that was given a value of 4.4, which is equivalent to an FR-4 epoxy when the loss tangent is 0.02.

Radar Cross Section (RCS) of a Metallic Plate

To examine the effects of the space-filling curve absorbing surfaces on the Radar Cross Section (RCS) of a metallic plate, a comparison of the RCS, both in the presence of as well as in the absence of the space-filling curve absorbing surfaces was conducted. A square metallic plate of dimensions 172 mm by 172 mm (see Figure 39) was modeled and the mono-static RCS of the plate, excited by a normally incident plane-wave polarized in the x-direction, is shown in Figure 40 as a function of frequency. The RCS of the metallic plate, in the absence of the space-filling curve surfaces, is compared with the cases in the presence of the space-filling curve surfaces utilizing a 15 mm thick substrate with real permittivity of 4.4 and a loss tangent of 0.08. The metallic plate, the finite substrate and the finite array of space-filling curves were all modeled using a commercially available Finite Element Method (FEM) code. For the above given

Figure 39: Geometries for RCS Comparison
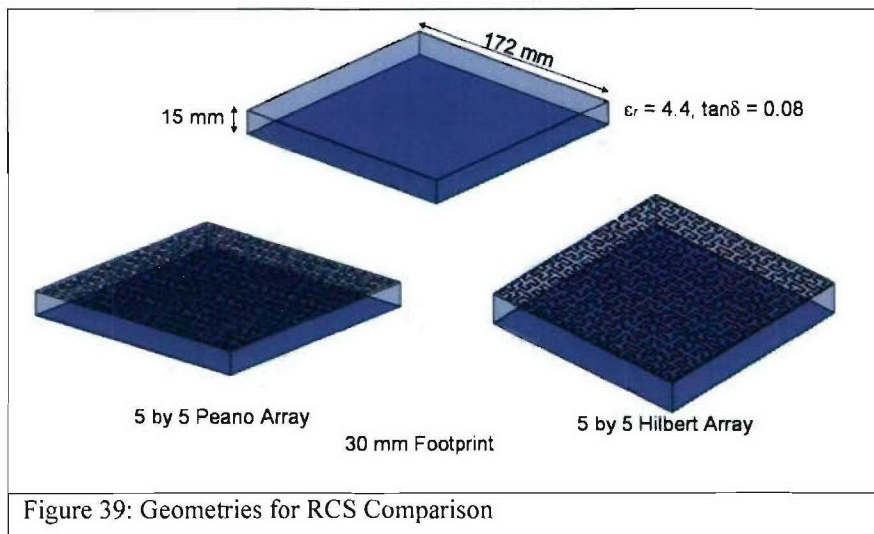
dimensions of the metallic plate, a 5 by 5 array of elements were utilized in order to cover the plate. The effects of the surface can be seen where the surfaces obtain resonance. For both cases involving the space-filling curve surfaces, the mono-static RCS of the conducting plate is significantly reduced.

Figure 40: Simulated RCS Comparison
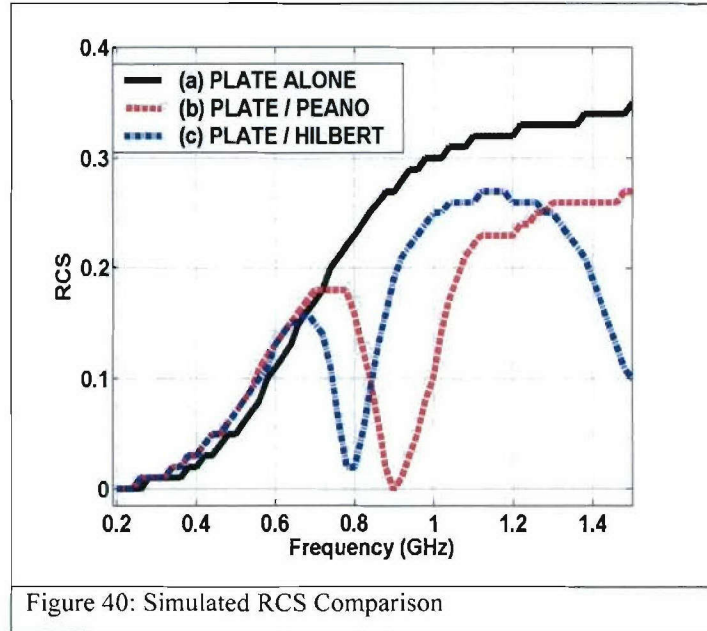
RCS Measurement

In order to confirm the theory, the RCS measurement of a metallic plate covered by the fabricated Hilbert surface of order 3, discussed in section 3.1, was carried out using an Agilent ENA5071B vector network analyzer and a pair of H-1479 horn antennas (1.0-12.4 GHz). The probe-to-probe distance between the horn antennas was approximately 10 inches. A 12 by 19 inch metallic plate was placed 10 feet downrange of the transmit and receive horn antenna pair. S12 was collected versus frequency for the metallic plate both in the absence of and in the presence of the fabricated Hilbert surface of order 3 (see Figure 41). The surface in this experiment is the same surface as presented in the waveguide measurement, in section 3.2 of this report, with the exception that the array now contains 19 by 23 elements. Where the Hilbert surface is present, a foam spacer was utilized to place the surface at a height of approximately 6mm above the metallic plate. The magnitude of S12 is shown in Figure 42, for the metallic plate alone and in the

presence of the Hilbert surface. As can be seen, the magnitude of the return signal is greatly reduced when the Hilbert surface is present, and this loss is primarily due to the effects of the loss tangent of the substrate, in the presence of the SF-Curve AMC surface.

Figure 41: Geometries for RCS Measurement Comparison

Figure 42: Measured RCS Comparison
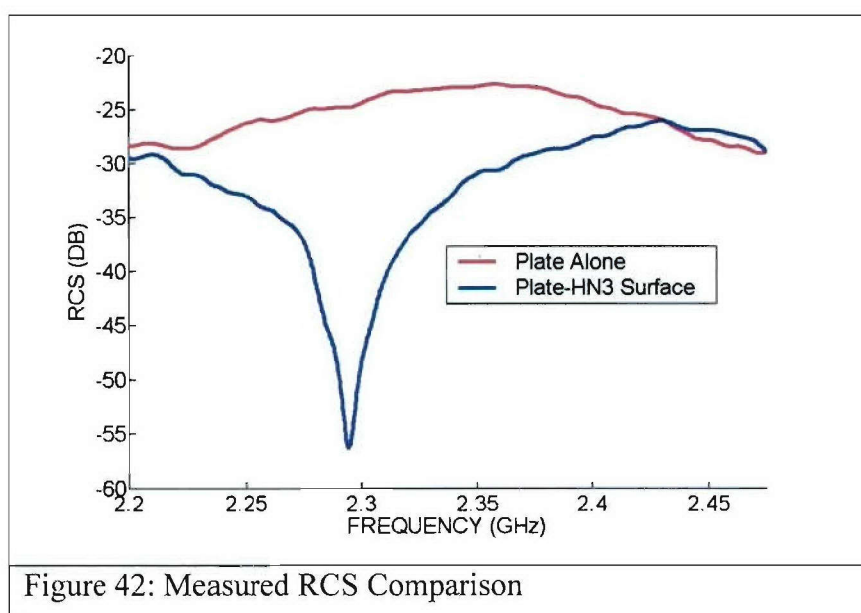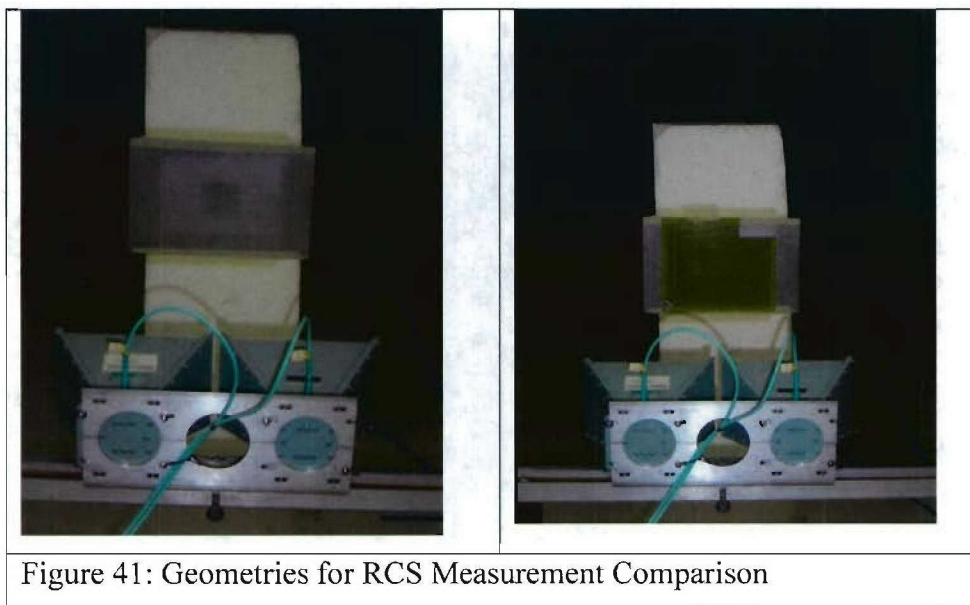
Polarization-Independent Thin Radar Absorbers

In many applications, the polarization dependence of such an absorbing surface would be considered unacceptable. In order to address the issue of the polarization dependence, each cell within the surface, which originally consisted only of a single inclusion, was altered such that each cell contained a 2 by 2 array of inclusions as is shown in Figure 43, and as was previously reported above. The diagonal elements in this sub-array are rotated 90° such that the surface reflection coefficient becomes identical for the Ex and Ey excitations. In Figure 43, it is shown that the reflection coefficient magnitudes are identical for the Ex and the Ey polarization cases and for this sub-array, the losses occur with no dependence on the polarization of the incident field.
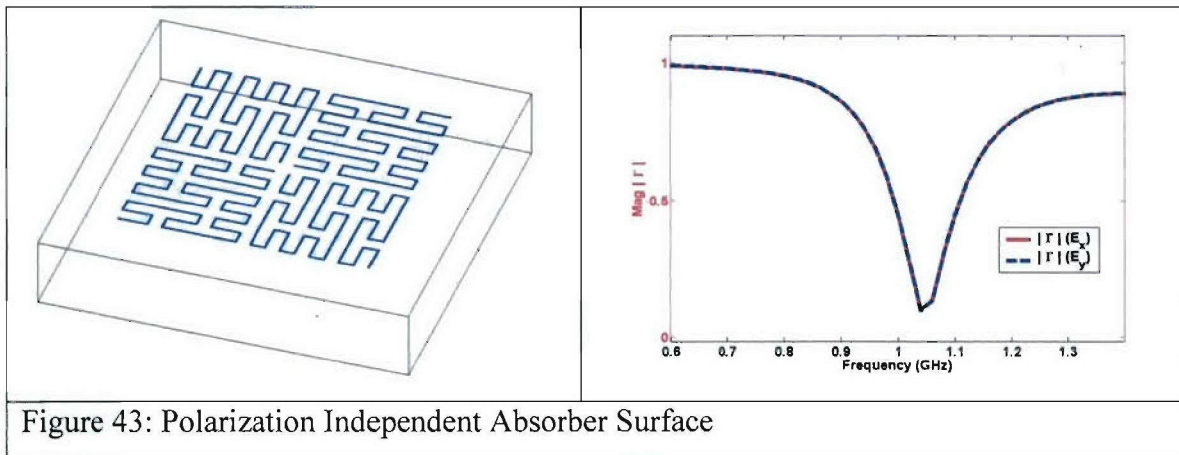

Figure 43: Polarization Independent Absorber Surface

5. Space-Filling Curve RFID Tags

Recently there has been considerable interest in the area of Radio Frequency Identification (RFID) and Radio Frequency Tagging (RFTAG). This emerging area of interest can be applied for inventory control (commercial) as well as friend/foe identification (military) to name but a few. The current technology can be broken down into two main groups, namely passive and active RFTAG's. This work focuses on the later, utilizing space-filling curves as a completely passive identification system.

The Peano and Hilbert space-filling curves have been shown to posses the ability to resonate at frequencies in which the overall footprint that the curve encompasses is relatively small with respect to the operational wavelength. This property may allow for a relatively small resonant passive tag with comparably large scattering characteristics. The relatively narrow bandwidth inherent to these geometries may prove to be useful in the spectral efficiency sense.

5.1 Single Peano and Hilbert Elements

The monostatic RCS as a function of frequency and the scattering RCS patterns for the single inclusion if free space is shown in Figure 44 for the case of the Peano curve element and in Figure 45 for the Hilbert curve element.

As can be seen, both curves posses resonances dependant on the polarization of the excitation and at the resonances, the curves behave like resonant dipoles, and yet the 30 mm x 30 mm footprint, which encloses these curves, is electrically very small with respect to the resonant wavelengths. Since the curves are smallest with respect to the first resonance, corresponding to the y-polarized electric field, this study will focus on this lowest resonance. The narrower bandwidth associated with this resonance will be utilized to pack a particular RCS signature within a relatively narrow band spectrum.
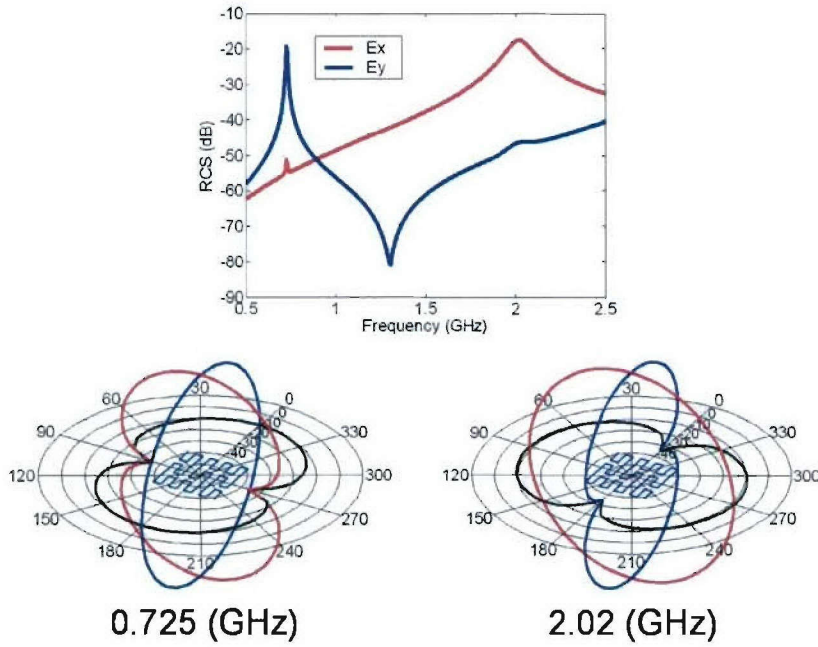
Figure 44: Monostatic RCS versus Frequency and RCS Patterns for a Single Peano Curve Element of Order 2, for Uniform Plane Wave Excitations with Differing Polarizations

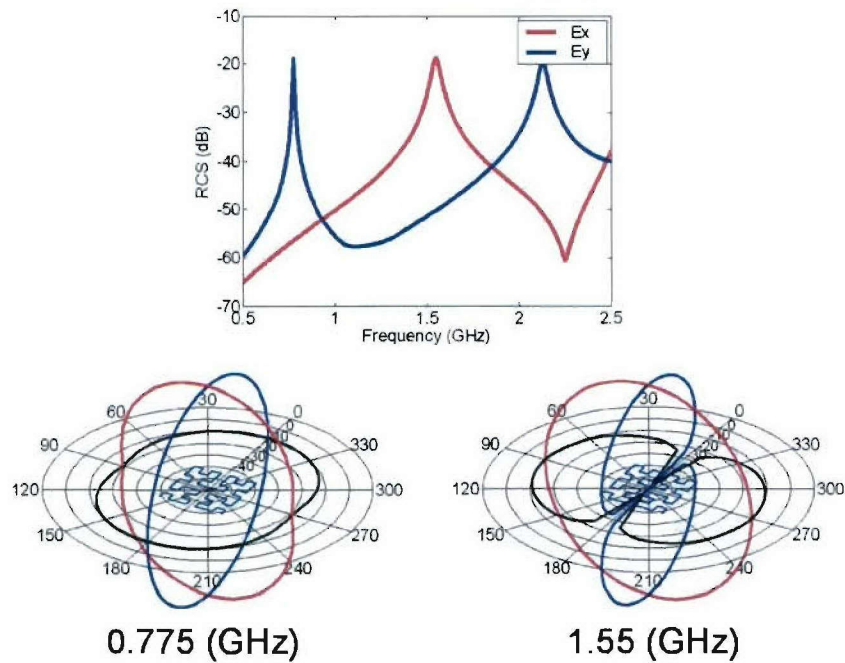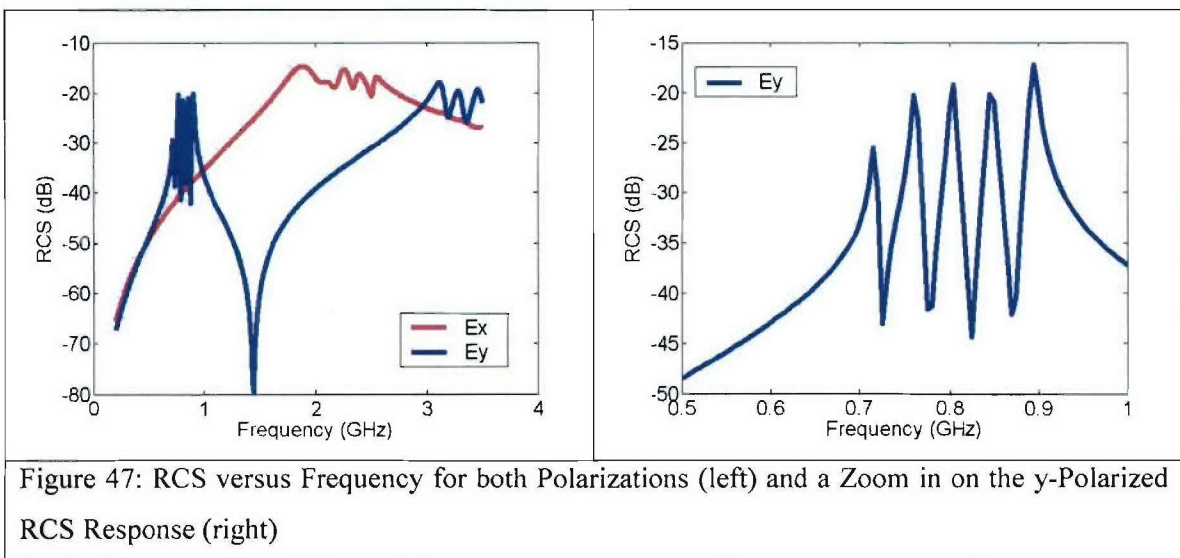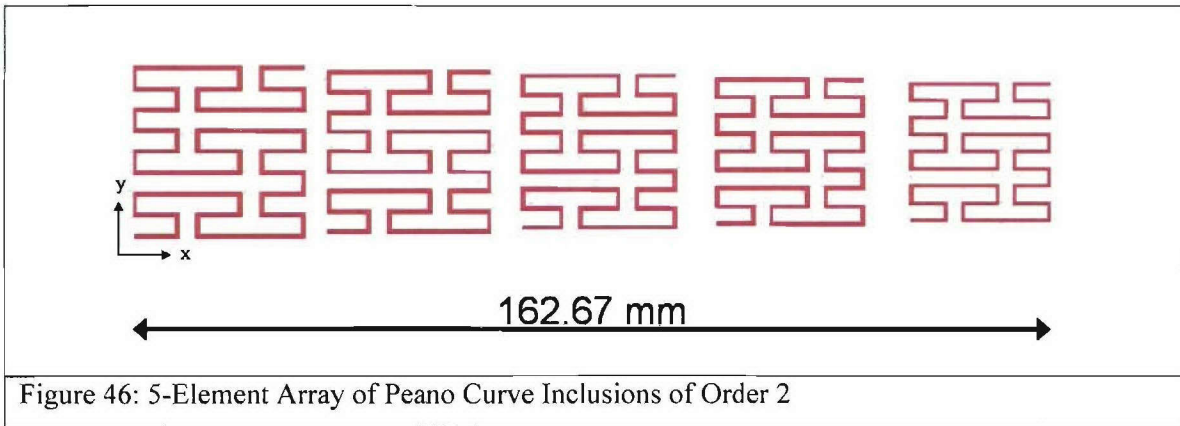0.725 (GHz)   2.02 (GHz)

Figure 45: Monostatic RCS versus Frequency and RCS Patterns for a Single Hilbert Curve Element of Order 3, for Uniform Plane Wave Excitations with Differing Polarizations

0.775 (GHz)   1.55 (GHz)

5.2 Five Element Arrays of Peano and Hilbert Elements

To illustrate a potential application, an array of Peano curve scatterers is shown in Figure 46. Each element within the array is designed to resonate at a separate and particular frequency. When illuminated with a normally incident plane-wave excitation, this geometry gives rise to the scattering shown in Figure 47. Multiple peaks in the Radar Cross Section (RCS) are evident and each peak corresponds to the resonance of a different element within the array. For this illustration, the array was designed to produce a monostatic RCS representative of the binary number 1101, where a peak in the RCS refers to a binary 1. For comparison, the corresponding Hilbert array and its scattering characteristics are shown in Figures 48 and 49, respectively.

Figure 46: 5-Element Array of Peano Curve Inclusions of Order 2

Figure 47: RCS versus Frequency for both Polarizations (left) and a Zoom in on the y-Polarized RCS Response (right)
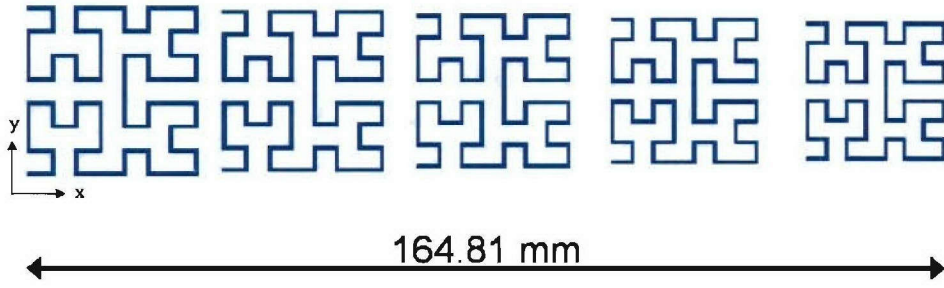
41

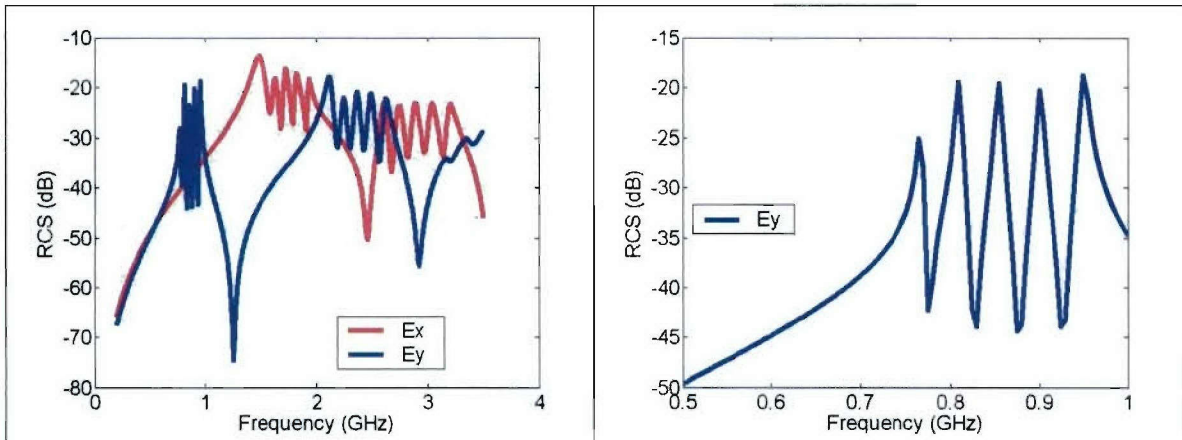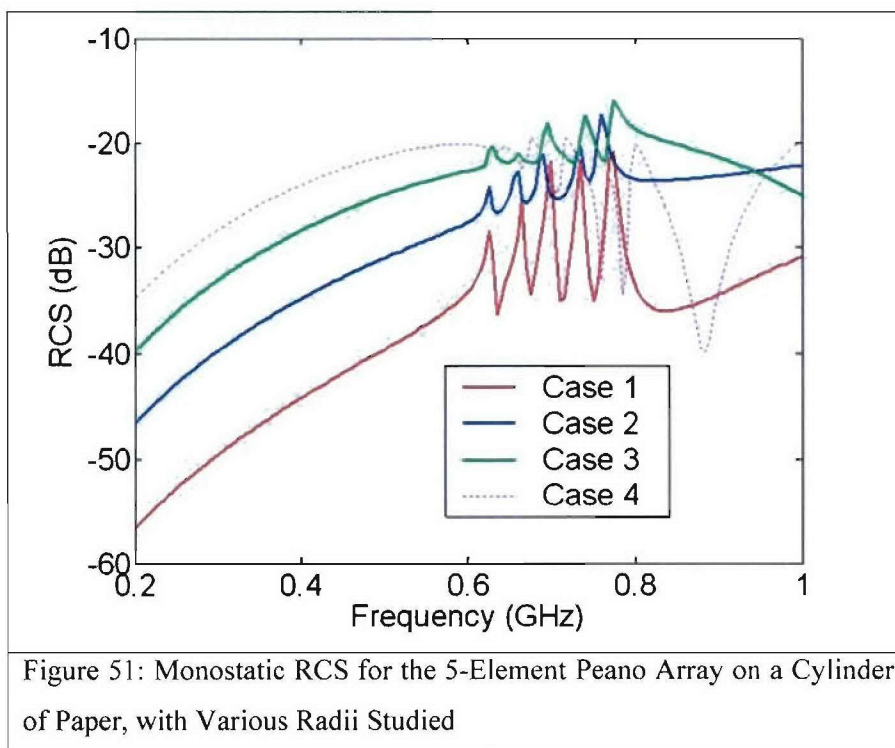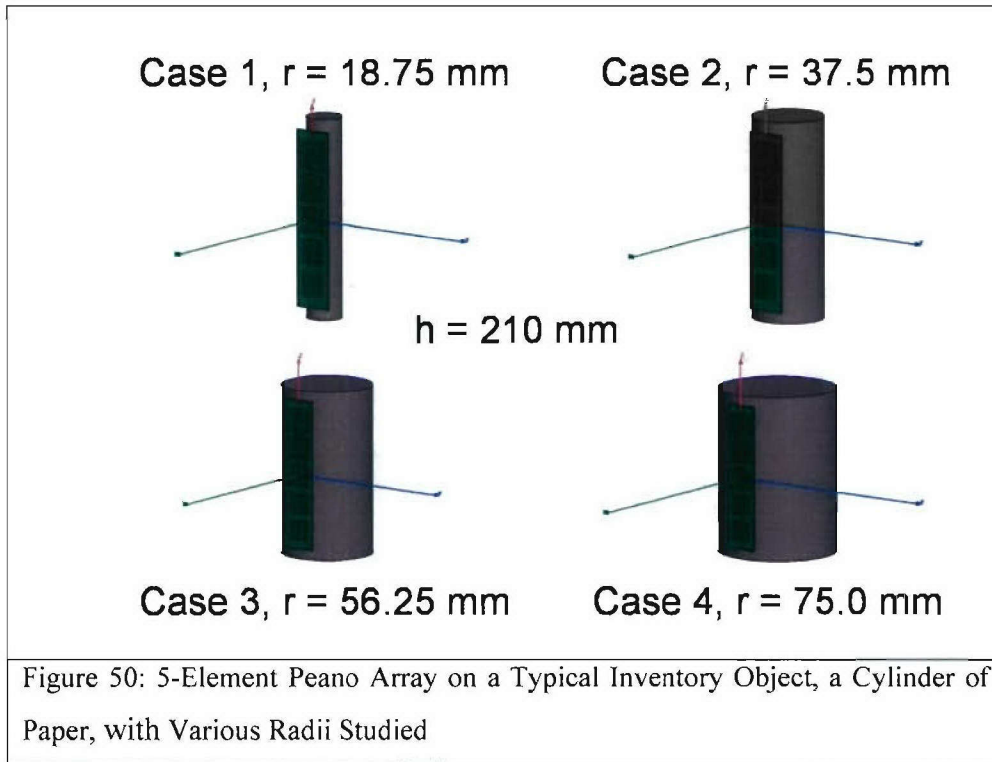Figure 48: 5-Element Array of Hilbert Curve Inclusions of Order 3

Figure 49: RCS versus Frequency for both Polarizations (left) and a Zoom in on the y-Polarized RCS Response (right)

## 5.3 Peano RFTAG on Dielectric and Conducting Cylinders

To investigate the performance of the proposed space-filling RF tags when placed near a typical inventory object, we have numerically modeled, using Finite Element Method (FEM), the RCS of the 5-element array of Peano-curve elements of 2nd order on a paper roll (see Figure 50). The paper roll was assigned $\varepsilon r = 2.6$, $\tan\delta = 0.08$ as given as appropriate values in [21]. The monostatic RCS results are plotted in Figure 51, for the paper rolls of various radii, as shown in Figure 50. One can clearly see the peaks corresponding to the resonant frequencies of the Peano curve elements. As the radius of the paper roll increases, however, the resonant peaks become less pronounced due to the increased contribution of the paper roll to the overall RCS of the combined geometry.

42

Appropriate signal processing algorithms may potentially be used to enhance the peaks in the received RCS spectrum.

Figure 50: 5-Element Peano Array on a Typical Inventory Object, a Cylinder of Paper, with Various Radii Studied

Figure 51: Monostatic RCS for the 5-Element Peano Array on a Cylinder of Paper, with Various Radii Studied

In a similar fashion, the Peano Array can be studied on a metallic object as well. In the cases depicted in Figure 52, the 5-Element Peano array was placed on an aluminum cylinder, and again, cylinders of different radii were studied.

The five peaks in the RCS, corresponding to the 5 separate resonant frequencies of the elements in the array are clearly evident for the smaller value of the cylinder radius but when the radius in increased, these peaks are lost in the dominant RCS return from the cylinder (see Figure 53). Techniques such as background subtraction as well as other possibilities to recover the signature from the RFTAG are currently under investigation, as well as fabrication and measurements, for experimental verification, all of which will be reported in future.

Figure 52: 5-Element Peano Array on an Aluminum Cylinder

Figure 53: Monostatic RCS for the 5-Element Peano Array an Aluminum Cylinder
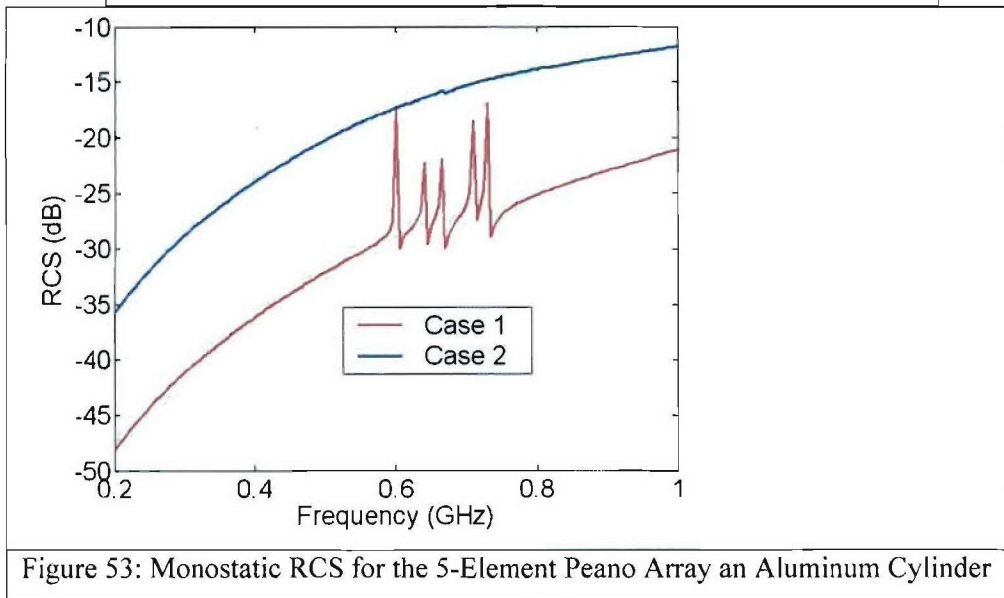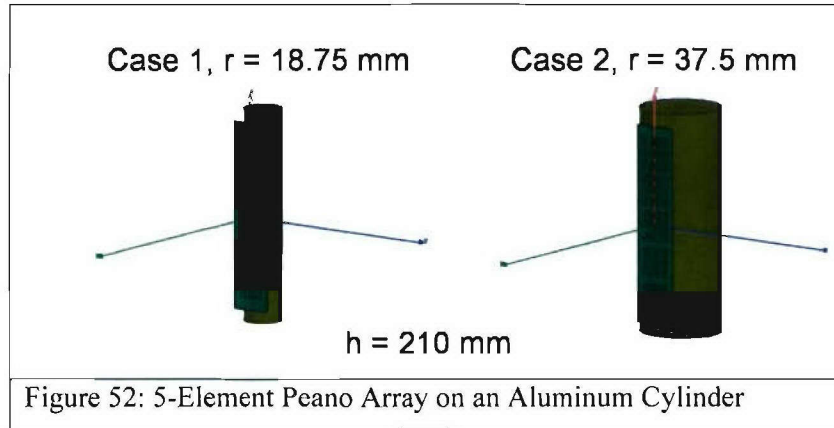
6. References

1. Hans Sagan, *Space-Filling Curves*, Springer-Verlag, 1994.

2. K. J. Vinoy, K. A. Jose, V. K. Varadan and V. V. Varadan, "Hilbert curve fractal antenna: a small resonant antenna for VHF/UHF applications," *Microwave and Optical Technology Letters,* Vol 29, No. 4, pp. 215-219, May 2001.

3. K. J. Vinoy, K. A. Jose, V. K. Varadan and V. V. Varadan, "Resonant frequency of Hilbert Curve fractal antennas," *Digest* of *the 2001 IEEE AP-S Internat. Symposium*, Boston, MA, pp. 648-652.

4. S. R. Best, "A comparison of the performance properties of the Hilbert curve fractal and meander line monopole antennas," *Microwave and Optical Technology Letters*, Vol. 35, No. 4, pp. 258-262, November 20, 2002.

5. K. J. Vinoy, K. A. Jose, V. K. Varadan and V. V. Varadan, "Hilbert Curve Fractal Antennas with Reconfigurable Characteristics," *Proceedings of the 2001 IEEE MMT-S Symposium*, Phoenix, AZ, pp. 381-384, 2001.

6. J. Zhu, A. Hoorfar and N. Engheta "Bandwidth, cross polarization, and feed-point characteristics of matched Hilbert antennas," *IEEE Antennas and Wireless Propagation Letters*; Vol. 2, pp. 2-5, 2003.

7. J. Zhu, A. Hoorfar and N. Engheta "Peano Antennas," accepted for *IEEE Antennas and Wireless Propagation Letters*. Vol. 3, PP. 71-74, December 2004.

8. C. A. Balanis, *Antenna Theory, Analysis and Design*, 2nd edition, 1997.

9. D. Rubin, *The Linville Method of High Frequency Transistor Amplifier Design*, Naval Weapons Center, NWCCL, TP 845, Corona Labs, Corona, CA, March 1969.

10. G. J.Burke and A. J. Poggio, "Numerical Electromagnetics Code (NEC)-method of moments," *Technical Document 11*, Naval Ocean Systems Center, San Diego, CA, September 6, 1982.

11. D. Sievenpiper, L. Zhang, R. F. Jimenez Broas, N. G. Alexopolous, and E. Yablonovitch, "High-impedance electromagnetic surfaces with a forbidden frequency band," *IEEE Transactions on Microwave Theory and Techniques*, Vol. 47, No. 11, pp. 2059-2074, November 1999.

12. F. Yang and Y. Rahmat-Samii, "Reflection Phase Characterization of an Electromagnetic Band-Gap (EBG) Surface," *Digest of the 2002 IEEE Antennas and Propagation Society International Symposium, San Antonio, Texas*, June 16-21, 2002, pp. 744-747, Vol. 3.

13. Y. Zhang, J. von Hagen and W. Wiesbeck, "Patch Array as Artificial Magnetic Conductors for Antenna Gain Improvement," *Microwave and Optical Technology Letters*, Vol. 35, No. 3, pp. 172-175, November 5, 2002.

14. R. Gonzalo, P. de Maagt, and M. Sorolla, "Enhanced patch-antenna performance by suppressing surface waves using photonic-bandgap substrates," *IEEE Trans. Microwave Theory & Tech.*, vol. 47, pp. 2131-2138, Nov. 1999.

15. R. C. Hansen, "Effects of a High-Impedance Screen on a Dipole Antenna," *IEEE Antennas and Wireless Propagation Letters*, vol. 1, pp. 46-49, 2002.

16. N. Engheta, "Thin Absorbing Screens Using Metamaterial Surfaces," Digest of the 2002 *IEEE AP-S International Symposium, San Antonio*, TX, June 16-21, 2002, pp. 392-395, vol. 2.

17. J. McVay, N. Engheta and A. Hoorfar, "High-Impedance Metamaterial Surfaces Using Hilbert-Curve Inclusions," *IEEE Microwave and Wireless Component Letters*, Vol. 14, No. 3, pp. 130-133, March 2004.

18. John McVay, Ahmad Hoorfar and Nader Engheta, "Applications of Hilbert Artificial Magnetic Conductor Ground Planes to Performance Enhancement of Electrically Small Antennas," *2003 IEEE Sarnoff Symposium*, March 11-12 2003, pp 297-300.

19. J. McVay, A. Hoorfar and N. Engheta, "Peano High Impedance Surfaces," *Radio Science*, Vol. 40, pp. 1-9, September 2005.

20. R. L. Fante and M. T. McCormack, "Reflection Properties of the Salisbury Screen," *IEEE Transactions on Antennas and Propagation*, Vol. Ap-36, 1988.

21. R. Olmi, M. Tedesco, C. Riminesi and A. Ignesti, "Thickness-independent measurement of the permittivity of thin samples in the X band," *Measurement Science and Technology*, Vol. 13, pp 503-509, 2002.

22. V. Jamnejad and A. Hoorfar, "Design of Corrugated Horn Antennas by Evolutionary Optimization Techniques," IEEE Antennas and Wireless Propagation Letters, Vol. 3, PP. 276-280, December 2004.

REPORT DOCUMENTATION PAGE

Form Approved
OMB No. 0704-0188

1. REPORT DATE (DD-MM-YYYY)	2. REPORT TYPE	3. DATES COVERED (From - To)
16/12/2005	Final	June 2004 - September 2005

4. TITLE AND SUBTITLE

Novel Electrically Small Antennas and Metamaterial High Impedance Surfaces

5a. CONTRACT NUMBER

5b. GRANT NUMBER
N00014-04-1-0619

5c. PROGRAM ELEMENT NUMBER

6. AUTHOR(S)

Hoorfar, Ahmad (PI)

5d. PROJECT NUMBER

5e. TASK NUMBER

5f. WORK UNIT NUMBER

7. PERFORMING ORGANIZATION NAME(S) AND ADDRESS(ES)

Villanova University - Center for Advanced Communications
800 Lancaster Avenue - Tolentine 119
Villanova, PA 19085

8. PERFORMING ORGANIZATION REPORT NUMBER
5-27726

9. SPONSORING/MONITORING AGENCY NAME(S) AND ADDRESS(ES)

Office of Naval Research
875 N. Randolph Street
12th Floor, One Liberty Center
Code 02
Arlington. VA 22217-5660

10. SPONSOR/MONITOR'S ACRONYM(S)
ONR

11. SPONSOR/MONITOR'S REPORT NUMBER(S)

12. DISTRIBUTION/AVAILABILITY STATEMENT

Approved for Public Release; Distribution is Unlimited

13. SUPPLEMENTARY NOTES

14. ABSTRACT

We have applied the mathematical concept of space-filling curves in design of electrically small planar antennas and in development of metamaterial high impedance surfaces (i.e., artificial magnetic conductors). In particular, our research has included the following areas: (i) Investigation of fundamental characteristics of matched off-center fed Space-Filling Curve (SF-Curve) radiating elements such as Hilbert curve and Peano curve antennas, and fabrication and measurement of a prototype to verify the theory; (ii) Analysis of mutual coupling effects between a pair of SF-curve antennas, and investigation of Yagi arrays made of Peano or Hilbert antenna elements; (iii) Analysis, fabrication and measurement of high-impedance surfaces, also known as artificial magnetic conductors (AMC), made of a periodic arrangement of Hilbert- or Peano curve inclusions; (iv) Application of SF-curve AMC surfaces in design of electrically thin microwave absorbers for RCS reduction; (v) Application of an array made of SF-curve resonating elements in design of novel RFID tags, and their performance analysis in RF tagging of dielectric and conducting cylindrical objects.

15. SUBJECT TERMS

Electrically Small Antennas, Space-filling Curves, Hilbert Antennas, Peano Antennas, High Impedance Ground-Planes, Artificial Magnetic Conductors, Thin Absorbers, RFID tags.

16. SECURITY CLASSIFICATION OF:			17. LIMITATION OF ABSTRACT	18. NUMBER OF PAGES	19a. NAME OF RESPONSIBLE PERSON
a. REPORT	b. ABSTRACT	c. THIS PAGE	UU		Dr. Ahmad Hoorfar
U	U	U			**19b. TELEPHONE NUMBER** (Include area code) 610-519-7223

Standard Form 298 (Rev. 8/98)
Prescribed by ANSI Std. Z39.18